Tailoring the Ignition and Reaction Properties of Cu_2O Thermite Nanolaminates

by

Lauren LeSergent

A thesis
presented to the University of Waterloo
in fulfilment of the
thesis requirements for the degree of
Masters of Applied Science
In
Mechanical Engineering- Nanotechnology

Waterloo, Ontario, Canada, 2018

Author's Declaration

I hereby declare that I am the sole author of this thesis. This is a true copy of the thesis, including any required final revisions, as accepted by my examiners.

I understand that my thesis may be made electronically available to the public.

Abstract

Thermites are a class of energetic material that produce heat through an exothermic reaction, making them useful for welding, metal refining, and propulsion applications. Compared to traditional micron-scale thermite powders, nanothermites offer improvements in the reaction rate, sensitivity, and activation energy. These nanothermites also offer structure and size dependent controllability of the reaction and ignition properties.

Due to the development of nanothermites, novel thermite applications have been proposed, including materials for micropropulsion, microwelding, and MEMs. For many of these applications, their feasibility depends on the controllability of thermite ignition and reaction characteristics, presenting a need for a more in-depth understanding of the controllability and reaction mechanisms of these materials.

In this work, the tunability of reaction and ignition characteristics of Al-Cu_2O thermite nanolaminates are explored through heating in a Differential Scanning Calorimeter, and with laser ignition. This serves to provide a basis for how structural parameters allow for the manipulation of reaction characteristics. Additionally, there are a lack of laser studies for aluminum-copper-based thermite nanolaminates, and this directly addresses the relationship between structural parameters and laser ignition/reaction parameters.

A novel method for determining the reaction mechanism of thermite nanolaminates is also introduced in this work. Understanding the reaction mechanism is vital when seeking to accurately model or design thermite nanomaterials, and this offers an alternative method to the common differential scanning calorimetry, thermogravimetric analysis, and transmission electron spectroscopy studies

Acknowledgement

I would like to acknowledge Prof. John Z. Wen and Prof. Carolyn Ren for their support and guidance. Their genuine enthusiasm for their research was motivating, and I truly appreciate them sharing their knowledge with me and encouraging me to pursue different interests and research angles.

I would also like to thank my committee members, Prof. Michael Mayer and Prof. Kevin Musselman for their valuable questions and comments, and their help with improving my manuscript.

I am grateful to have had the opportunity to collaborate with many colleagues and researchers, and I would like to thank the current and past members of the Laboratory for Emerging Energy Research (LEER) for their valuable input and help. I have had the honor of collaborating with Hongtao Sui, Florin Saceleanu, Dr. Sanam Atashin, Gurkan Yesiloz, and Pei Zhao, and am grateful for their time and assistance. Yiqi Zhang has been most helpful with providing her expertise for modeling laser absorption using Lumerical software, and I would like to thank her for providing these models. I would also like to extend my gratitude to Catalin-Florin Petre, Daniel Chamberland, Pascal Béland, and Tommy Ringuette for their help with laser ignition testing, and for sharing their knowledge with me.

I have received incredible support during the past years, and would like to thank my family, friends, and boyfriend for believing in me, providing encouragement, helping during the rough times, and for offering guidance. I am truly lucky to have all of you. Special thanks to Patrick Chen and Peach for always cheering me on.

Dedicated to my sister, Morgan.

Table of Contents

List of Figures

List of Tables

Abbreviations

AES- Auger Electron Spectroscopy

AFM- Atomic Force Microscopy

ALD- Atomic Layer Deposition

DSC – Differential Scanning Calorimetry

DFT- Density Functional Theory

DTA- Differential Thermal Analysis

EDX - Energy Dispersive X-ray Spectroscopy

EPD- Electrophoretic Deposition

FIB- Focussed Ion Beam

FTIR- Fourier-Transform Infrared Spectroscopy

HR-TEM- High Resolution Transmission Electron Microscopy

IR- Infrared

LEIS- Low-Energy Ion Scattering Spectroscopy

MEMS – Microelectromechanical Systems

RBS- Rutherford Backscattering Spectroscopy

SEM – Scanning Electron Microscopy

STEM- Scanning Transmission Electron Microscopy

TEM – Transmission Electron Microscopy

TGA – Thermogravimatric Analysis

Tof-MS- Time-of-Flight Mass Spectrometry

XPS – X-ray Photoelectron Spectroscopy

XRD - X-ray Diffraction

1. Introduction

1.1 Motivation and Problem Statement

Thermites are energetic materials that produce heat through an exothermic reduction-oxidation reaction between a metal and an oxide. Aluminum is most commonly used as a fuel in combination with CuO, Fe_2O_3, and NiO. However, other metals and oxides can include magnesium, boron, silicon, zinc, titanium, MoO_3, WO_3, and Bi_2O_3.

Due to their high heat release, thermites are used for applications such as metal refining, munitions, and welding. And, newly proposed uses include initiators for MEMs systems, materials for micropropulsion, and materials for microwelding [1] [2] [3]. For these newly proposed applications, the controllability of the reaction characteristics –such as initiation temperature, heat release, stability, burn rate, gas generation, and flame velocity – become even more important, as well as understanding their reaction mechanism.

Nanothermites are a class of thermite materials whose components have at least one dimension that is at the nano scale (< 1 μm) in size. Due to their small size and resulting large specific surface area, they offer a decrease in the activation energy, an increase in the reaction speed, and an increase in sensitivity. These factors offer considerable improvements over the traditional micro-scale thermites, and offer size and structure dependent controllability of reaction properties. These characteristics have led to considerable interest in the field of nanothermite science and technology. In particular, thermite nanolaminates have gained interests due to their large interfacial area, ease of modeling, improved homogeneity, compatibility with MEMS, and high degree of structural controllability.

Given the importance of gaining a more in-depth understanding of thermite materials, for the development of new technologies, it is vital to explore how physical and chemical characteristics affect the thermite reaction. Additionally, it is important to determine the reaction mechanism, and understand how physical and chemical characteristics can be used to tailor the properties of nanothermites to suit future applications.

1.2 Research Objectives

The objectives of this thesis are to synthesize Al-Cu_2O thermite nanolaminates and to investigate the factors controlling their reaction characteristics. Importance will be placed on how the structural characteristics such as layer thickness, number of layers, overall thickness, layer order, and use of a copper interlayer, affect the reaction characteristics. Additionally, a novel method for examining the reaction mechanism of thermite nanolaminates will be developed, and will be included to help explain reaction phenomena. Through this, conclusions will be drawn about how structural manipulation can be used to tailor the reaction characteristics of thermite nanolaminates to suit future applications.

1.3 Thesis Organization

A literature review, including an introduction to thermite chemistry, a discussion of applications, and a discussion on fabrication methods, will be given in Chapter 2. Chapter 3 provides a description of the methods and equipment used during this study. The development of a novel method for determining the reaction mechanisms of thermite nanolaminates will be outlined in Chapter 4, and used to provide a theoretical reaction model. Chapters 5 provides a discussion on how the structural characteristics affect the ignition and reaction characteristics using differential scanning calorimetry. The effect of structural properties on the ignition and reaction characteristics

for laser ignition is given in Chapter 6. Finally, Chapter 7 will provide a summary of the effects of structural characteristics, and will discuss future directions.

2. Literature Review

This chapter provides a description on the current research on nanothermite composition, applications, fabrication methods, and classification. The advantages of nanothermites over microthermites are considered, and the benefits of using nanolaminates are presented. The thermite compositions of Al-CuO, Al-Cu_2O, Al-Fe_2O_3, and Al-NiO will be discussed briefly, before a more in-depth analysis of Al-CuO and Al-Cu_2O thermites are provided. The need for more Al-Cu_2O research will also be established. Some of the current applications and fabrication methods will be introduced, and the merits of the different fabrication methods will be compared. A brief discussion on the important parameters when characterizing thermite reaction will be given. Finally, the specific research gaps and goals of this study will be outlined and related to current work.

2.1 Introduction to Thermite Materials

Thermites are energetic materials that produce heat through an exothermic reduction-oxidation reaction between a metal and an oxide. In this reaction, the oxide is reduced by the metal fuel, due to the oxygen and metal forming stronger more stable bonds. This reaction is shown below, where M represents the fuel (metal or alloy), AO is the oxide, A is a metal or non-metal produced during the thermite reaction, and MO is the oxide produced during the thermite reaction. Heat is generated during this process, and ΔH represents this heat of reaction.

$$M + AO \rightarrow MO + A + \Delta H \quad (1)$$

For the thermite reaction to initiate, two events need to occur. First, a sufficient amount of energy needs to be transferred to the sample in order to overcome the initial activation energy barriers of the thermite reaction. Second, a mass transfer of active components to the interface, and through any protective oxide layers, must ensue. Therefore, thermite ignition and reaction can

be discussed in terms of heat and/or mass transfer, and thermite improvement can occur through optimizing these factors

Traditional thermites consisted of mixed microscale powders due to their low cost and ease of production, and due to the lack of development of nanotechnology. These powders had high energy densities, but slow reaction speeds compared to other energetic materials, which affected their time dependent power densities [4]. Additionally, microscale thermites are less sensitive to ignition by impact, friction, heat, and electrostatic discharge, making it difficult to ignite them [5].This made microscale powder thermites less ideal for applications requiring high power density and facile ignition. However, it was found that decreasing the length scale of the thermites led to an increase in the reaction speed, and a decrease in the activation energy [6]. This was attributed to the fact that decreasing the size of the particles led to an increase in the surface to volume ratio, which increases the interfacial area through which the reaction occurs, and leads to a decrease in the diffusion distance for mass transport [6]. Additionally, nanopowder mixtures are generally more homogeneous and have better contact between particles. These factors led to a higher ignition sensitivity and higher reactivity. For example, 20-50 nm Al and MoO_3 powder mixtures reacted over 1000 times faster than the traditional thermite powders [7]. It was also found that shrinking powders to the nanoscale was able to decrease the melting temperature of Al by as much as 300 K [6].

The development of nanolaminates further increased the improvements made by nanopowders versus traditional powders. These structures are composed of nanolayers of metals and oxides, and have large interfacial regions between each layer. Due to their small layer thickness, and large interfacial area, they offer further improvements on the surface to volume ratio and mass transport. Additionally, because of the increased contact between reactive components (flat

layered geometry versus packed-sphere geometry) the reaction can proceed more readily [4]. Figure 2-1 illustrates the increase in publishing for nanolaminates and nanothermites from 2005-2017, showing the growing interest of the scientific community. The publication numbers were obtained by searching “nanolaminates” and “nanothermites” using Scopus research database, and sorting by publication year.

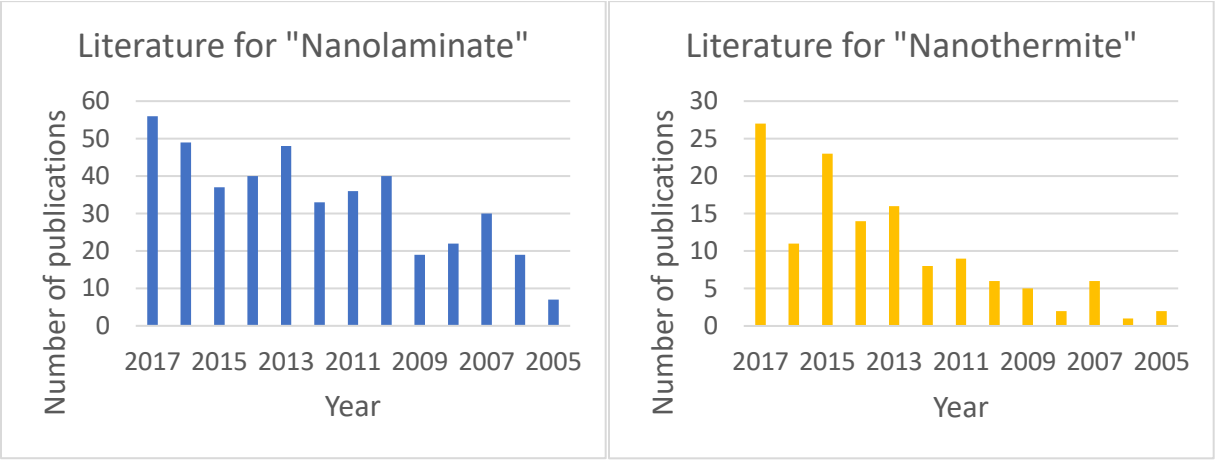

Figure 2-1 Increase in publications on nanolaminates and nanothermites from 2005-2017

Figure 2-2 provides an illustrated comparison of traditional micropowders, nanopowders, and nanolaminates. It can be noticed that decreasing the powder size has increased the surface to volume ratio and decreased the mass transport distance. Additionally, by changing the geometry from packed-sphere to nanolaminate, the interfacial area between the reactive components increases.

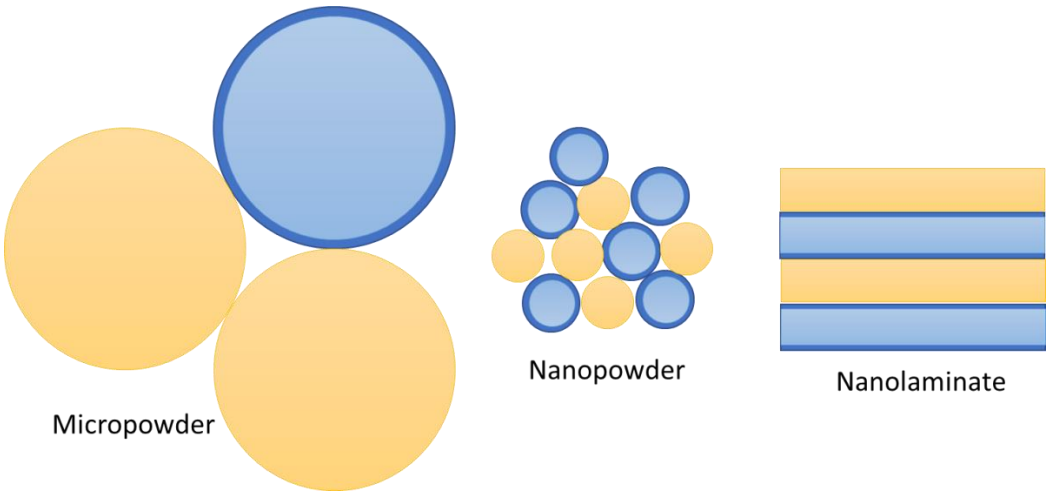

Figure 2-2 Comparison of micro and nano powders and nanolaminates

2.2 Composition

As mentioned in the previous section, thermites consist of metal and oxide components that undergo an exothermic reduction-oxidation reaction. The metal can be aluminum, zinc, boron, titanium, magnesium, or silicon. The oxide can be, but is not limited to, CuO, Fe_2O_3, NiO, MoO_3, WO_3, Bi_2O_3, and Cu_2O. Since the driving force of the thermite reaction is due to the difference between the formation enthalpies of the reactant and product oxides [8] [4], the exothermic reaction can be tailored by material choice alone. Table 2-1 shows a comparison of the heat of reaction, adiabatic reaction temperature, and gas production for selected thermites: Al-CuO, Al-Cu_2O, Al-Fe_2O_3, Al-NiO. In this case, aluminum-based thermites were selected since they are highly studied, aluminum is an abundant material, they have high reactivities, they form a protective oxide layer that improves the stability of pure aluminum, and they are relatively safe with benign reaction products [9].

Table 2-1 Properties of selected thermites, modified from Fischer et al. [10]

	Heat of reaction (cal/g)	**Adiabatic reaction temperature (K)***	**Gas production (g gas/g reactants)**
2Al + 3CuO	974.1	5718	0.3431
2Al + $3Cu_2O$	575.5	4132	0.0776
2Al + Fe_2O_3	945.4	4382	0.0784
2Al + 3NiO	822.3	3968	0.0063

*The adiabatic reaction temperatures listed here are without consideration to phase changes

The amount of gas produced during the reaction can play a role in the explosiveness of the material, and can also affect the quality and strength of welds and joins due to the generation of bubbles and pores. It is generally accepted that low-gas production is best for welds and, as Al/NiO has significantly lower gas production than Al/CuO, Al/Cu_2O, and Al/Fe_2O_3, it has been suggested for welding and joining applications [11]. It should be noticed that the "gas production" given in the table refers to gas produced in reference to the total mass of reactants. This explains why the gas production for Cu_2O is significantly lower than CuO. As shown by equations (2) and (3), for a complete reaction, the ratio of CuO to Al by weight is approximately 4.4:1, whereas the ratio of Cu_2O to Al by weight is approximately 8:1. Given this, the amount of active Al in a stoichiometric Al-Cu_2O thermite is approximately half that of the amount of Al in a stoichiometric Al-CuO thermite, leading to a lower heat of reaction (2434 J/g vs 4067 J/g [12]), and a lower gas production in reference to total reactant mass.

$$3Cu_2O + 2Al \rightarrow 6Cu + Al_2O_3 + \Delta H \quad (2)$$

$$3CuO + 2Al \rightarrow 3Cu + Al_2O_3 + \Delta H \quad (3)$$

From Table 2-1, the Al-CuO thermite has the highest heat of reaction, which illustrates its high energy release compared to the other materials. This factor, along with the ability to control gas release, makes CuO an extremely well-studied thermite, both theoretically and experimentally. Relative to Al-CuO thermites, Al-Cu_2O thermite has received much less attention, and have been the focus of considerably fewer studies. This is surprising given that Al-Cu_2O thermites also have tunable gas release, and that the reaction between Al and Cu_2O is an intermediate step for the reaction of Al-CuO thermites. This is shown below in the series of equations (5)-(13), which illustrate all the possible reactions, decompositions, and phase transformations occurring for the overall Al-CuO thermite reaction shown by equation (4). These equations are modified from Baijot et al. [13]

$$3CuO + 2Al \rightarrow 3Cu + Al_2O_3 \quad (4)$$

$$2CuO_{(s)} \leftrightarrow Cu_2O_{(s)} + \frac{1}{2}O_{2(g)} \quad (5)$$

$$Cu_2O_{(s)} \rightarrow Cu_2O_{(l)} \quad (6)$$

$$Cu_2O_{(l)} \leftrightarrow 2Cu_{(l)} + \frac{1}{2}O_{2(g)} \quad (7)$$

$$Cu_{(s)} \rightarrow Cu_{(l)} \quad (8)$$

$$Cu_{(l)} \leftrightarrow 2Cu_{(g)} \quad (9)$$

$$Al_2O_{3(s)} \rightarrow Al_2O_{3(l)} \quad (10)$$

$$2Al_{(g)} + \frac{3}{2}O_{2(g)} \leftrightarrow Al_3O_{3(l)} \quad (11)$$

$$Al_{(s)} \rightarrow Al_{(l)} \quad (12)$$

$$Al_{(l)} \leftrightarrow Al_{(g)} \quad (13)$$

Equation (5) shows the reversible decomposition/recombination of the CuO/Cu_2O bulk materials. Equations (6) and (7) represent the phase change and decomposition of Cu_2O, which produces gaseous oxygen and Cu. The phase changes of Cu from solid to liquid, and from liquid to gas are shown in equations (8) and (9). Equations (10) and (11) represent the phase change of the alumina, and the reversible decomposition/combination of the Al_2O_3/Al and oxygen. Finally, equations (12) and (13) represent phase changes of the Al. It should be noted that the oxygen utilized in the thermite reaction, for the oxidation of Al, can come from CuO or Cu_2O, as shown by equations (4) and (6). Thus, it is necessary to gain an understanding of the Al/Cu_2O reaction and initiation characteristics. It is an important intermediate reaction, and helps with gaining an understanding of the overall Al-CuO reaction mechanism.

The published studies on Al-Cu_xO_y (where x and y are integers that represent the oxide type: CuO, Cu_2O, and Cu_3O_4) thermite nanolaminates, as well as the study types, are displayed in Table 2-2. Most of these studies aim to optimize/classify the material behaviour, while a few propose and investigate the reaction mechanisms. It should be noted that, out of all these studies, only one focusses on Al-Cu_2O nanolaminates, and it does not provide an in-depth discussion on the reaction model, highlighting the shortage of research for this thermite type. Additionally, none of these studies provide an in-depth discussion on laser ignition of Al-Cu_xO_y thermite nanolaminates. Therefore, there is a literature gap of studies on the laser ignition, heat-ignition, and reaction mechanism of Al-Cu_2O thermite nanolaminates. The purpose of this study is to address these identified gaps in literature.

Table 2-2 Published studies on aluminum-copper-based thermite nanolaminates

Study Type	Year	Material	Reference
Experimental (TEM, STEM, AFM, profilometry, XRD)	2018	Al/CuO	[14]
Experimental (photodiode, high speed camera) and theoretical (2D diffusion-reaction modeling)	2017	Al/CuO	[15]
Experimental (DSC, XRD, high speed camera, emission spectroscopy, pyrometry)	2017	Al/Cu_2O/Cu	[16]
Experimental (photodiode) and theoretical (1D ignition model based on thermal exchange and atomic diffusion)	2017	Al/CuO	[17]
Experimental (XRD, DSC, TGA, TEM, STEM)	2017	Al/CuO	[18]
Experimental (nanocalorimetry, high speed camera, Tof-MS)	2017	Al/CuO	[19]
Experimental (DSC, XRD, STEM, HR-TEM,)	2016	Al/CuO/Cu	[20]
Experimental (TEM, STEM, IR spectroscopy, XPS, LEIS, DSC, high speed camera, FTIR) and theoretical (DFT)	2015	Al/CuO/Cu	[21]
Experimental (SEM, high speed camera)	2015	Al/CuO	[22]
Experimental (ToF-MS, high speed camera, SEM) and theoretical (1D diffusion model)	2015	Al/CuO	[23]
Experimental (TEM, XRD, DSC)	2014	Al/CuO	[8]
Experimental (HR-TEM, STEM, XPS, XRD, DSC, high speed camera)	2014	Al/CuO	[24]
Experimental (FTIR, HR-TEM, profilometry, XRD, ellipsometry, XPS, DSC) and theoretical (DFT)	2013	Al/CuO	[25]
Experimental (SEM, XRD, DSC, high speed camera, temperature diagnosis system)	2011	Al/CuO	[26]
Experimental (SEM, TEM, AFM, XRD, FTIR, profilometry, DSC, DTA)	2010	Al/CuO	[3]
Experimental (high speed camera)	2010	Al/CuO	[27]
Experimental (XRD, TEM, AES, XPS, DTA, photodiode)	2003	Al/CuO_x	[28]
Experimental (XRD, TEM, AES, XPS, DTA)	2003	Al/CuO_x	[29]
Experimental (AES, XPS, RBS)	1991	Al/CuO	[30]

2.3 Applications

One of the largest industrial uses for thermites is welding, due to the large amount of heat produced during the exothermic reaction. Iron-based thermites, in particular, are a commonly used material for welding railway rails. In this reaction, the produced heat creates a melt of Fe and Al_2O_3

materials. Due to the differences in density, the molten iron will sink, and it can be poured from the bottom of the container to form the weld. The Al_2O_3 will collect at the top as slag material, and is generally not used for the weld. It should also be noted that thermite can be used for underwater welding since it cannot be easily extinguished by water [31]. Additionally, since the oxygen necessary for reaction is contained within the oxide, thermites could also be used for welding in low-oxygen environments or vacuum, leading to proposed uses for spacecraft maintenance.

Thermites can be used in metal refining given that, during the thermite reaction, the metal fuel is oxidized to form an oxide, and the reacting oxide is reduced to form a metal. This can result in the formation of a pure metal from it corresponding oxide. For example, to extract chromium from a Fe-Cr alloy, sodium chromate is first formed by heating the ore with sodium carbonate [32]. Then, heat and sulfur are added to form sodium sulfate and a chromium oxide. This oxide can then be reduced to pure chromium by undergoing a thermite reaction. It should be noted that, in some cases, it is difficult to separate the created metal from the oxide matrix. This imposes limits on the use of thermites for metal refining.

Materials for propulsion and thrust is an area of thermite research that uses the energy and/or gas generated from thermite reactions to produce movement, and can be applied to a large variety of applications. For example, Hacker et al. discussed the use of thermites for high-speed propulsion of underwater vehicles. This involved utilizing a thermite fuel to vaporize water, and create motion by using it in a high-pressure jet [33]. Gash et al. tested the performance of thermite nanolaminates as a component in mock M55 detonators, which are a type of detonator used for mortars and rockets [34]. And, Apperson et al. evaluated the thrust performance of nanothermites for thrusters that could be applied as a means of course correction for microsatellites and high-velocity projectiles [35]. For this application, it is crucial that the actuation time be as brief as possible to

prevent the thrust vector from rotating as the projectile spins [1], which is well suited to nanothermites due to the controllability of their reaction and ignition times. The integration of thermite materials with MEMs further improves their capacity for thermites to be used for novel micropropulsion and microthruster applications since this allows for precise amounts of thermite to be activated separately.

Thermite can also be applied to a number of novel and developing uses. It can be used medically to generate pressure pulses to aid in cell transfection, gene transfer, and drug delivery [36]. It can be incorporated into MEMs devices for spot-heating and pressure pulse generation. Additionally, a nanothermite composite was proposed as a novel detector for dark matter [37].

2.4 Fabrication Methods

Given the vast array of thermite structures and applications, many methods can be employed for thermite fabrication. These include, but are not limited to, ball milling, sonication, sputtering [16] [25] [17] [15] [14] [21], atomic layer deposition (ALD) [25] [38], electrospraying [39] and electrospinning [40], sol-gel synthesis [41], vacuum filtration [42], electrophoretic deposition (EPD) [43] [44], polymer-directed assembly [45], and even DNA directed assembly [46].

Sonication involves mixing metal and oxide particles in a solvent, and using sound waves to provide agitation. In contrast, traditional ball milling involves using a rotating cylindrical container full of grinding media (typically metal or ceramic balls), where the motion and impact of the grinding media causes mixing and a reduction in particle size. Both of these mechanical mixing methods are scalable and inexpensive. However, contamination from solvents or grinding media can be an issue, highly-ordered structures cannot be produced, and it is difficult to create homogeneous mixtures [47]. For ball-milling methods, there can be a range of sizes and

morphologies in powders prepared this way, making reproducibility an issue. Additionally, ball milling can also pose safety risks, due to the possibility of premature ignition from the impact and friction occurring during these processes. For highly reactive mixtures, this method is not recommended.

Sol-gel processing is a technique of thermite manufacturing that generally creating a porous metal-oxide structure from solution, and metal particles can be added during or after the formation of the gel. It is easy to produce thermite with this method, since it requires little equipment, and offers an inexpensive way to provide good contact between reactants. However, this method has issues with impurities from the sol-gel process, which can cause significant decreases in performance, and it is difficult to control or change the structures [47].

Novel methods such as DNA-directed assembly, polymer-based assembly, and the use of surface modifiers to promote assembly, can ensure an almost homogeneous mixture of metal and oxide particles. They are generally inexpensive, easy to scale (depending on method), and are controllable. However, the polymers, biomolecules, and modifiers used provide a very large amount of impurities compared to other methods [47]. Figure 2-3 provides an illustration, from Séverac et al., of the process utilized to produce DNA-directed thermite nanocomposites [46]. In this method, Al and CuO nanoparticles were functionalized with complimentary single-stranded DNA, which formed nanocomposites when mixed.

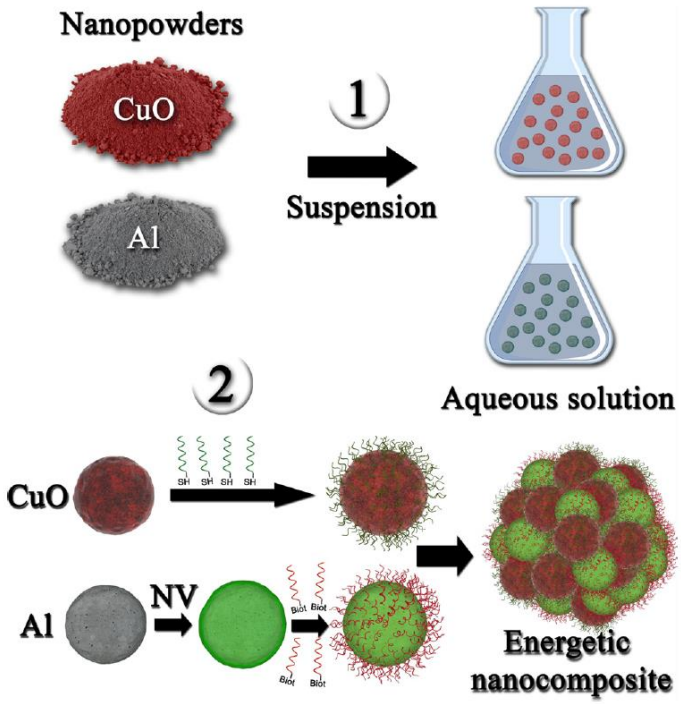

Figure 2-3 Process of DNA-directed self assembly, reproduced from Séverac et al [46]

Electrospraying and electrospinning generally involves mixing thermite particles in a colloidal solution, and electrospinning/electrospraying the solution so that fibers of thermite material are formed. Figure 2-4, from a study by Yan et al, shows a comparison of fibers containing no nanoparticles, <50nm Al nanoparticles, and <50nm Al and CuO nanoparticles [40]. These methods are able to create novel materials such as energetic fibers and fabrics, and are a relatively easy and scalable process. However, impurities, difficulties with obtaining homogeneous particle mixtures, and lack of intimate contact between the reactants are issues that should be considered.

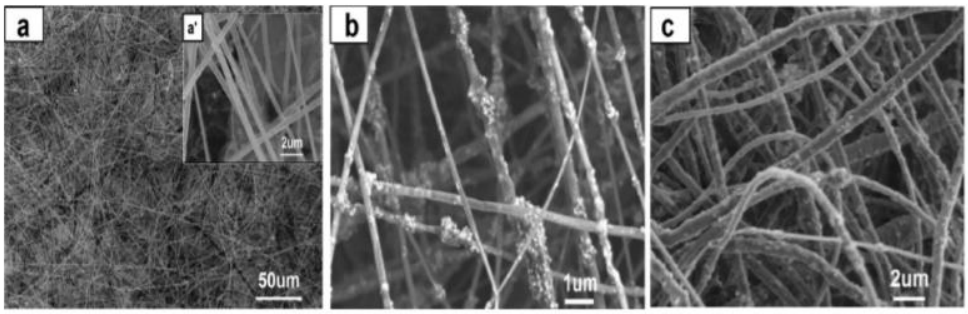

Figure 2-4 SEM images of nitrocellulose with a) no nanoparticle addition, b) 50 wt% <50nm Al particles and c) 50 wt% <50nm Al and CuO particles, reproduced from Yan et al. [40]

Electrophoretic deposition and vacuum filtration can create structures with thick layers of particles. These layers can be mixed (containing both the oxide and metal nanoparticles within the same layer), or unmixed (each layer contains either metal particles or oxide particle). These are inexpensive methods and easy to scale. However, they are unable to create very thin layers (usually on the scale of micrometers instead of nanometers), and the interfaces aren't uniform. When creating dense mixed-particle materials, they can have similar problems to thermites produced through physical mixing. Additionally, EPD can be limited in terms of compatible materials, since materials must be able to carry a charge and be stable in suspension, and adding materials to help with stability/charge can lead to impurities. Figure 2-5 shows a layered structure created through the vacuum filtration method of Sui et al [42]. These layers are microscale, and are difficult to decrease to the nanoscale using this method.

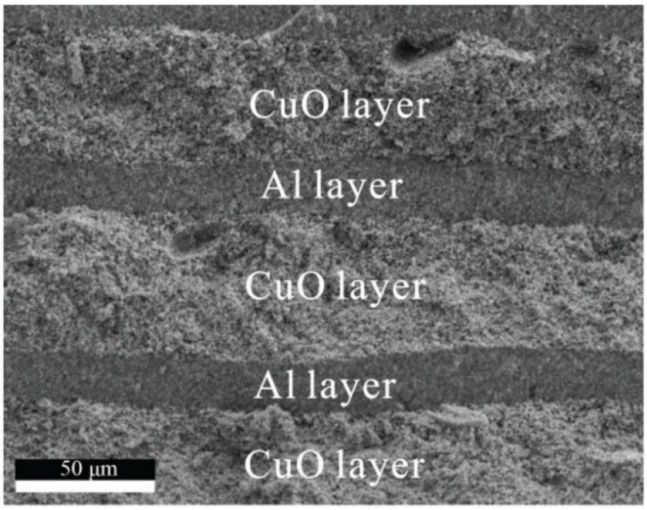

Figure 2-5 Layered structure created through vacuum filtration, from Sui et al [42]

Methods that are capable of producing nanolayered thermites, such as sputtering and ALD, offer improvements on homogeneity. ALD involves the use of a gas phase material to selectively deposit layers of material on the substrate. As illustrated in Figure 2-6, the gases react with the substrate so that the material is absorbed to form a thin layer. By controlling the number of exposures and precursor types, layered structures can be created with an exceptionally high degree of uniformity and structural control.

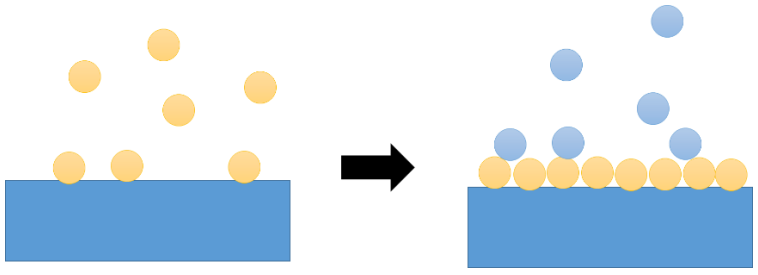

Figure 2-6 Illustration of the ALD process for creating layered materials

Sputtering involves the use of a negatively charged target in a controlled gas environment. The negative charge causes free electrons to leave the target, and collide with the gas to create positively ionized gas. There positive ions, attracted to the negatively charged target, can then bombard the target and "sputter" off material. The material can deposit on the substrate of choice, and the substrate is typically rotating throughout deposition to ensure a more uniform coating. Argon is most commonly utilized as the gaseous species during sputtering, due to it being inert and heavy enough to cause ionization more easily that lighter inert gases. However, gases such as oxygen can also be utilized to create metal oxides from pure metal targets, due to the fact that some of the oxygen can be incorporated into the material depositing on the substrate. Sputtering offers many advantages over the previous methods since it offers highly controllable layer thicknesses, and it is able to deposit most commonly used metal and oxide combinations for thermites. Also, due to its simple geometry and well-defined interfaces, it is easy to model and provides highly repeatable structures. However, problems with scalability, implementation costs, and potential instabilities from strain and interfacial free energies have prevented the widespread use of nanolaminates [47].

Table 2-3, adapted from X. Zhou et al. [47], provides a comparison between mechanically mixed, sol-gel produced, self-assembled, and sputtered methods for creating thermite materials. There methods were compared on the cost of production and equipment, the scalability of the process, the level of impurities, the safety concerns of the method and materials, the controllability of the nanostructure, and of the ease of integration of these materials with MEMs devices. Although sputtering is high cost and difficult to scale, it has the lowest impurity level, a high degree of safety, low environmental impact, excellent controllability, and is an ideal candidate for integration with MEMs. It is also the easiest structure to model, and can be produced easily under vacuum (reducing

undesirable effects/reactions from humidity or oxidation). As this study aims to investigate various factors controlling the reaction and initiation characteristics, and utilize a new method to determine the reaction mechanism of nanolaminates, the purity and controllability of the nanostructure is important. Therefore, sputtering was chosen as the ideal approach since it is highly controllable, can deposit a variety of materials, can easily coat different substrates, is easy to model, and can be done in a range of pressures, temperatures, and gas-environments.

Table 2-3 Comparison of selected preparation methods, modified from X. Zhou et al. [47]

	cost	**scalability**	**impurities**	**safety**	**Nanostructure controllability**	**MEMS integration**
Mechanically mixed	low	easy	high	Medium concern	Not controllable	Difficult
Sol-gel	low	easy	high	Precaution needed	Somewhat controllable	Difficult
Self-assembly	usually low	easy	high	Medium concern	Good controllability	Difficult
sputtering	high	difficult	Very low	Very safe	Excellent controllability	Easy

2.5 Classifying Thermite Reactions

As this study focusses on the controllability of thermite nanolaminates for the developing applications of micropropulsion, microwelding, and MEMS, it is important to understand the key parameters influencing their use. Therefore, this section aims to discuss the important parameters and terminology when classifying thermite reactions. This section also aims to highlight the importance of having a solid understanding of the reaction mechanism.

The ignition delay is a parameter that can be defined differently depending on the ignition system being used. Loosely stated, the ignition delay refers to the time interval between the

beginning of the heating event and the beginning of the exothermic reaction. For example, when utilizing laser ignition, the ignition delay can be calculated as the time difference between the laser illumination of the sample and the beginning of light emission from the sample (produced due to the exothermic reaction). This characteristic has been shown to decrease for nanothermites compared to microthermites [48]. It is an extremely important parameter for applications in microthrusters [49] or munitions primers, where the length of the ignition delay could impact the final vector of motion.

The ignition temperature refers to the temperature that must be reached in order for the activation energy barrier to be passed, and for the thermite reaction to begin. In differential scanning calorimetry (DSC) studies, this is generally defined as the temperature at which the exothermic reaction peak begins. Nanoscale thermites have shown to have lower melting temperatures compared to their microscale counterparts, allowing for some control over the ignition temperature. Control over this characteristic is important as it allows for a decrease in the required energy input, while also ensuring that the reaction temperature is high enough to impart stability and reduce the risk of unplanned combustion of the samples.

The average energy release refers to the amount of energy produced during the reaction interval, and is normalized by the sample mass since it is a mass dependent property. For DSC studies, the average energy release can be determined by integrating the exothermic reaction peak. Whereas, for laser ignition studies, this value can be determined by integrating the photodiode signal. The energy release if an important parameter since it will influence the applications that the thermite can be used in. For example, in joining applications, it is beneficial if the thermite material has a high enough energy release to melt the metals in the join area [9].

The reaction speed is important as it can influence the power density of a reaction. For high power applications, such as propellants, a fast reaction speed is typically ideal [50]. As mentioned previously, nanothermites offered an improvement on microthermites due to an increase in reaction speeds.

Finally, although not specifically a thermite parameter, it is vital to have a solid understanding of the reaction mechanism in order to accurately obtain meaning from experimental data and create models. Thermites can follow a condensed phase reaction mechanism, where the reaction occurs between two solid components. In contrast, the heterogeneous reaction mechanism involves the decomposition of the oxide to release gaseous oxygen, which then reacts with the solid metal. These mechanisms will be discussed in more depth in Section 4.0.

Unfortunately, determining the reaction mechanisms for thermites can be difficult due to the energetic nature of the thermite reaction. High heat production, particle sprays, pressure waves, and metal vapors from the exothermic reaction can damage equipment and lenses, leading to restrictions for equipment use. Previous research has mainly studied the reaction mechanisms utilizing TEM, DSC, or TGA data. However, DSC and TGA have limitations in characterizing complex structures since nanoscale materials behave differently than microscale materials, and their melting and reaction temperatures can be influenced by particle or layer size, the ability to form alloys, and the formation of oxides. DSC and TGA mainly provide an indirect method for determining the reaction mechanisms, since the mechanism is pieced together from the exothermic/endothermic peaks and mass loss, and can be subject to errors in interpretation. In contrast, TEM allows for direct viewing of the reaction, and can provide an in-depth analysis. However, access to a TEM capable of imaging energetic samples can be difficult and costly to obtain.

To limit the scope of this study, the parameters of ignition delay and ignition temperature, and the determination of the reaction mechanism, for both laser and DSC ignition, will be the main focusses of this work. However, some discussion on the rate of initial energy transfer and the average energy release will also be provided.

2.6 Current Research Gap and Goals

As mentioned in Section 2.2, out of all the Al-Cu_xO_y nanolaminate studies, only one focusses directly on Al-Cu_2O. This has resulted in a critical knowledge gap for the following reasons. Firstly, during the reaction of CuO with Al, it decomposes to form Cu_2O. It was shown that this produced Cu_2O can also participate in the reaction with Al, and this intermediate could affect the reaction characteristics. Therefore, it is vital to understand the reaction characteristics and mechanism of Al-Cu_2O in order to gain an understanding of the full picture for Al-CuO. Secondly, Al-Cu_2O has different properties than other aluminum-copper oxide based thermites, and needs to be classified.

In section 2.5 it was mentioned that determining the reaction mechanism of thermite materials is difficult due to their energetic nature, and that the current methods of TEM and DSC/TGA can be costly or prone to interpretation error. Therefore, there is a drive to produce a cheap, accessible, and reliable method of determining the reaction mechanism (or to use alongside other methods for further validation) for thermite nanolaminates. There is room for development in this area.

Laser has become a promising ignition source due to the tunability of its wavelength, tunability of its power density, and the ability to be focussed to change the spot size. Laser also offers a high degree of compatibility with MEMs technology, micropropulsion, and microwelding. However, very few laser ignition studies of thermite nanolaminates exist, and no laser ignition of thermite Al-CuxOy nanolaminates have been performed. Given the promise of this ignition source, the

popularity of Al-CuxOy thermites, and the lack of research in this area, this has become another critical research gap.

To address these gaps, three projects were proposed. Project one developed a unique method to characterize the nanolaminate reaction mechanism using gas capture and storage. The purpose was to not only develop an alternative method of determining reaction mechanisms, but to provide information on the reaction mechanism of Al-Cu_2O nanolaminates. The second project reacted Al-Cu_2O nanolaminates through heating in DSC and TGA, and provide an analysis of how structural properties affect the reaction and ignition characteristics. This addresses the lack of Cu_2O research, which is vital to improve our understanding of the popular Al-CuO reaction. Project 3 examines the laser ignition of Al-Cu_2O thermite nanolaminates, and discusses how structural factors affect the ignition and reaction properties. This directly address the lack of laser ignition research in this area.

3. Synthesis and Characterization of Al-Cu_2O Thermite Nanolaminates

This chapter outlines the synthesis method, factors affecting substrate choice, and characterization equipment for the thermite nanolaminates. Sputter deposition is introduced to fabricate the samples, and the settings and procedure will be briefly discussed. The choice of substrate can have a large effect on the reaction and ignition characteristics through its thermal conductivity, optical properties, reactivity, melting point, malleability, and diffusivity, and the effect of these properties will be presented. Finally, the various characterization equipment utilized in this study will be introduced.

3.1 Sputter Deposition of Nanolaminates

To create the well-defined layers of the thermite nanolaminates, Magnetron sputtering (AJA International, ATC Orion 5) was used, as shown in Figure 3-1. Prior to deposition, the substrate was cleaned and loaded into the machine chamber. The chamber was then pumped-down, using a vacuum pump, till a pressure below 1mTorr was reached. This was applied to ensure that contamination or reactions with air or humidity were avoided.

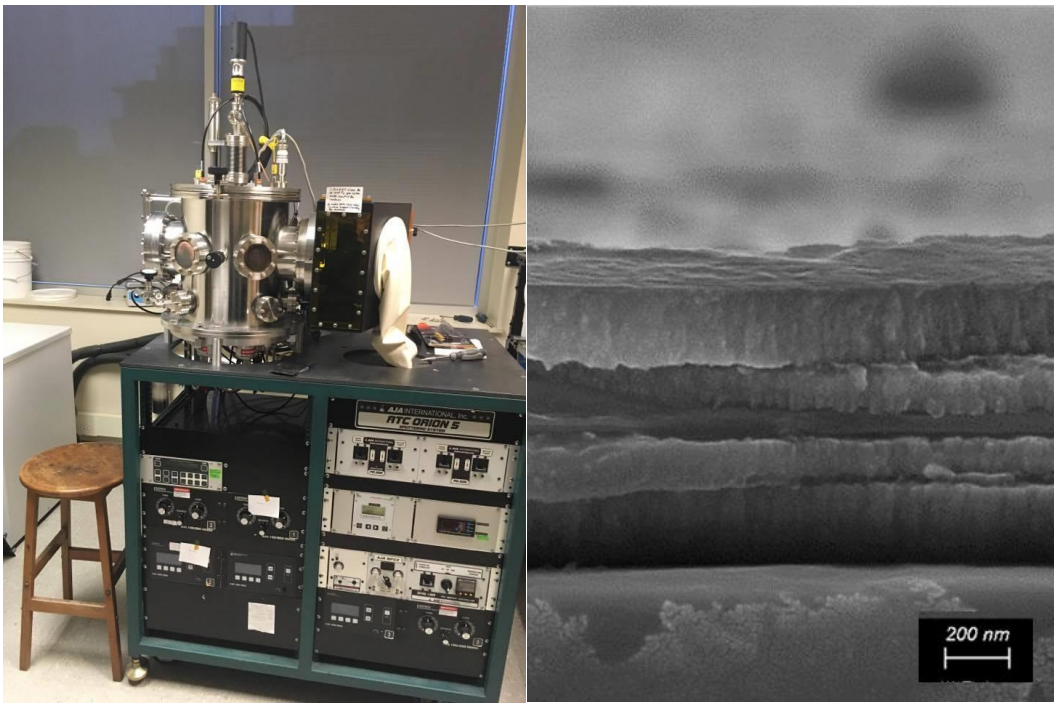

Figure 3-1 (left) the magnetron sputtering machine and (right) an SEM image demonstrating the layered structure produced

Two metal targets were used to create the layers of the thermite structures. To produce a pure Al layer, the Al target (AJA International Al target) was sputtered using Ar plasma (83W, 0.17 cm^3/s flow rate of Argon, and 0.53 Pa chamber pressure). To produce a pure Cu layer, the Cu target (AJA International Cu target) was sputtered using an Ar plasma (55W, 0.17 cm^3/s flow rate of Argon, and 0.53 Pa chamber pressure). And, finally, to produce the Cu_2O layer, the Cu target was sputtered using an Ar-O_2 plasma (55W, 0.08 cm^3/s flow rate for each Ar and O_2 gas, and 0.53 Pa chamber pressure). For the Cu_2O layers, in particular, the flow rates and chamber pressure were carefully calibrated to ensure that the correct copper oxide was attained (instead of CuO or Cu4O3). This calibration involved varying the pressure and flow rate ratios, and used XPS to ensure that the layer was Cu_2O (See section 3.3.7 for details on the XPS).

The sputtered layer thicknesses were controlled by varying the deposition time, and the deposition rates were determined using Dektak (See Section 3.3.3 for details on the Dektak) . For this, the materials were applied to silicon substrates for different deposition times (10, 20, and 30 mins), multiple thickness measurements were taken using the Dektak, and a relationship between deposition time and film thickness was drawn.

A more detailed description on the substrate preparation and sputtering process is given in Appendix A.

3.2 Substrate Effects

Due to mechanics of sputtering, where material from a target is ejected and deposited on a substrate, it is important that the substrate material characteristics be considered. These characteristics include the substrate thermal conductivity, melting temperature, malleability, reactivity, diffusivity, and optical properties (transmission, reflection, and absorption).

The thermal conductivity of the substrate material is important since it can impact the thermite ignition and reaction propagation [17] [27]. For example, for thin thermite layers, a highly conductive substrate can cause quenching of a reaction, or even stop the ignition process. This is due to the fact that thermite ignition requires an adequate amount of heat to be applied, and that the propagation of the reaction requires that any produced heat be adequate to start the reaction in neighboring material. For a highly conducting material, heat can be transferred away from the reaction site too quickly, resulting in a quenching of the reaction. Additionally, a highly conductive substrate can transfer heat away from an ignition site, preventing adequate heat build-up to initiate the reaction.

The melting temperature and malleability of the substrate are important given that these substrates will undergo heating during the initiation and reaction processes of the thermite materials. A substrate that maintains its structural integrity during the ignition and reaction temperatures is usually ideal. However, the proposed novel method (see Section 4.0 for details) for determining the reaction mechanism of thermite nanolaminates relies on the choice of a substrate that becomes sufficiently malleable during the heating process.

The reactivity and diffusivity of the substrate is another important consideration. The substrate should not contribute to the thermite reaction or have side-reactions with any components, thus contributing inaccuracies to results and models. The substrate atoms should ideally have poor diffusion in the thermite materials (and vice versa), to prevent mixing of the components. Additionally, the nanolaminate should have good adhesion to the substrate.

Finally, the optical properties such as transmission, reflectance, and absorption, become important when using lasers for ignition. If the thermite nanolaminates are sufficiently thin, light can pass through and interact with the substrate. In this case, it may be ideal to have a substrate with high absorption, and low reflectance and transmission, to maximize power absorption and heating at the thermite-substrate interface. In some cases, if igniting the sample from beneath, a substrate with very high transmission is required. These optical properties will also change with wavelength, so materials should be selected specifically for the light source.

In some cases, there may not be an appropriate substrate choice, so free-standing film or pellets can be fabricated. In this case, the samples are sputtered on top of a layer of photoresist, which can be dissolved in acetone. This produces free-standing layered flakes in solution, and they can be collected and used (freely or pressed into a pellet) for testing. Figure 3-2 shows the nanolaminate

film during the photoresist dissolving process (left), and after complete removal from the substrate (right).

Figure 3-2 The sputtered structures (left) during the dissolving process for the photoresist layer, and (right) the free-standing structures after being removed from their substrate

3.3 Characterization Methods

3.3.1 SEM/EDX

Scanning Electron Microscopy (SEM) was used to image the samples on the nano and micro-scale, and measure the layer thicknesses, and the built-in Energy Dispersive X-ray Spectrometer (EDX) was used for elemental analysis. For this, a Zeiss SEM with EDX was used. To prepare the samples for imaging, they were mounted on the SEM stages with carbon tape and coated with a thin gold layer to improve the conductivity.

3.3.2 DSC/TGA

Differential Scanning Calorimetry (DSC) and Thermogravimetric Analysis (TGA) are thermal analysis tools that were used to provide information on the thermite ignition temperature, heat release, and activation energy. For these tests, a NETZSCH STA 449 F3 Jupiter machine was used to collect thermal data, and the accompanying NETZSCH Proteus Thermal Analysis (version 6.1.0)

software was utilized for data analysis. The heating rates were set at 5, 10, 20 K/min, for a temperature range of 30-800 °C. The tests were performed under argon flow, to ensure that the oxygen utilized in the reaction is coming directly from the sample, and the rates were set at 0.08 or 0.17 cm^3/s. For some cases, the argon flow was changed to air to determine how the thermite materials reacted in the presence of environmental oxygen.

3.3.3 XPS

X-ray Photoelectron Spectroscopy (XPS) was used to determine the oxide type (CuO, Cu_2O, etc.) by looking at the oxidation state of the material. For this, a Thermo Scientific ESCALAB 250 XPS, with a built in Focused Ion Beam (FIB), was used. Measurements were taken of the surface, and then the FIB was used to remove surface layers to allow for measurements of the bulk. CasaXPS software (version 2.3.18PR1.0) was used to find the peaks, and the NIST X-ray Photoelectron Spectroscopy Database was used to determine the oxidation states based on peak position.

3.3.4 High Speed Camera

A high-speed camera was used to view the thermite reactions, determine the ignition delay, and determine the initial flame propagation velocity. For this, a Photron Fastcam SA1.1 high speed camera was used, along with the Photron Software Package (3.6.9), and was operated at 100,000 fps. By analyzing the video clips, the ignition delay can be determined by finding the difference between the time when the laser hits the sample and the time when ignition of the sample first appears. This will be discussed in further detail in Section 6.2 and Figure 6-2. In addition to this, observing the flame spread, in the first moment upon ignition, can be used to find the flame spread velocity. See Section 6.2 and Figure 6-3 for further details of how the flame spread varied with time.

3.3.5 Photodiode

An Osram SFH206K photodiode was used to determine the ignition delay and energy release. The energy release can be found by analyzing the time-averaged photodiode signal, and normalizing by the sample mass. The ignition delay was found by measuring the linear portion of the photodiode signal between laser illumination and the exothermic reaction. Further details on the ignition delay will be given in Section 6.2 and Figure 6-2.

3.3.6 Dektak

Dektak was used to perform thickness measurements, which were used to provide information on the deposition rate of the different materials. For this, a Veeco Dektak 8 stylus profilometer was employed. When gathering thickness data, multiple measurements were taken, and the averaged value was used to account for slight non-uniformities in film thickness.

3.4 Summary

In this chapter, the fabrication, substrate effects, and characterizations methods were presented. Sputter deposition was the method of choice for this study, as it was able to create nanoscale layer of Al and Cu_2O. For the Al layers, sputtering was done in an argon environment. However, for the Cu_2O layers, oxygen was introduced to ensure that the materials sputtered from the Cu target formed an oxide on the substrate.

The considerations of optical properties, diffusivity, reactivity, thermal conductivity, melting point, and malleability when choosing an appropriate substrate were discussed. Since Projects 2 and 3 are focused on how the structural characteristics of the nanolaminates affect the reaction properties, substrate effects should be minimized. Thus, the nanolaminates are removed from their substrates, once the sputtering process is complete, and tests are done on free-standing flakes or

pellets. For Project 1, the malleability of the substrate is important and, thus, glass is chosen due to its softening during heating in an oven.

An outline of the characterization methods was provided. SEM and high-speed camera allowed for imaging of the samples and reactions, while XPS, EDX, and dektak were used to provide information on the composition and thickness. DSC, TGA, and photodiode data provided information about the reaction and ignition characteristics.

4.0 Determination of the Reaction Mechanism of Al-Cu_2O Nanolaminates

To gain a strong understanding of the impact of structural properties on the ignition and reaction characteristics, it is important to first understand the underlying reaction mechanism of the Al/Cu_2O nanolaminates. However, as mentioned in Section 2.5, it can be difficult to determine these mechanisms due to the energetic nature of thermite materials. The high heat, pressure waves, particle sprays, and metal vapors produced during the reaction can be damaging, and limits the equipment that can be used for characterization. DSC and TGA have been used in literature, but they are an indirect method of determining the reaction, and can be subject to interpretation errors. While, TEM allows for direct viewing of the reaction, but access can be difficult or costly. Therefore, the development of an alternate method for determining the reaction mechanism would be beneficial to this research field.

Thermite reactions can occur through condensed phase or heterogeneous reaction mechanisms, as shown in Figure 4-1. In the condensed phase reaction scheme, the reaction occurs between two solid reactants, and ions are transported across the interface to initiate the reaction between the metal and the oxide. Whereas, for heterogeneous reactions, a decomposition of the oxide produces gaseous oxygen. This gaseous oxygen accumulates at the metal-oxide interface, and the thermite reaction occurs as the gas-phase oxygen oxidizes the metal fuel. In general, it is accepted that most nanothermite reactions occur through the condensed phase reaction pathway [51] [52] [53] [54] [55]. Nanolaminates, in particular, are dominated by condensed phase reactions [29] due their large interfacial area and high levels of contact between reactive components. However, there are exceptions to this general rule, and wrongly classifying the reaction mechanism can lead to inaccuracies in modeling and fundamental understanding.

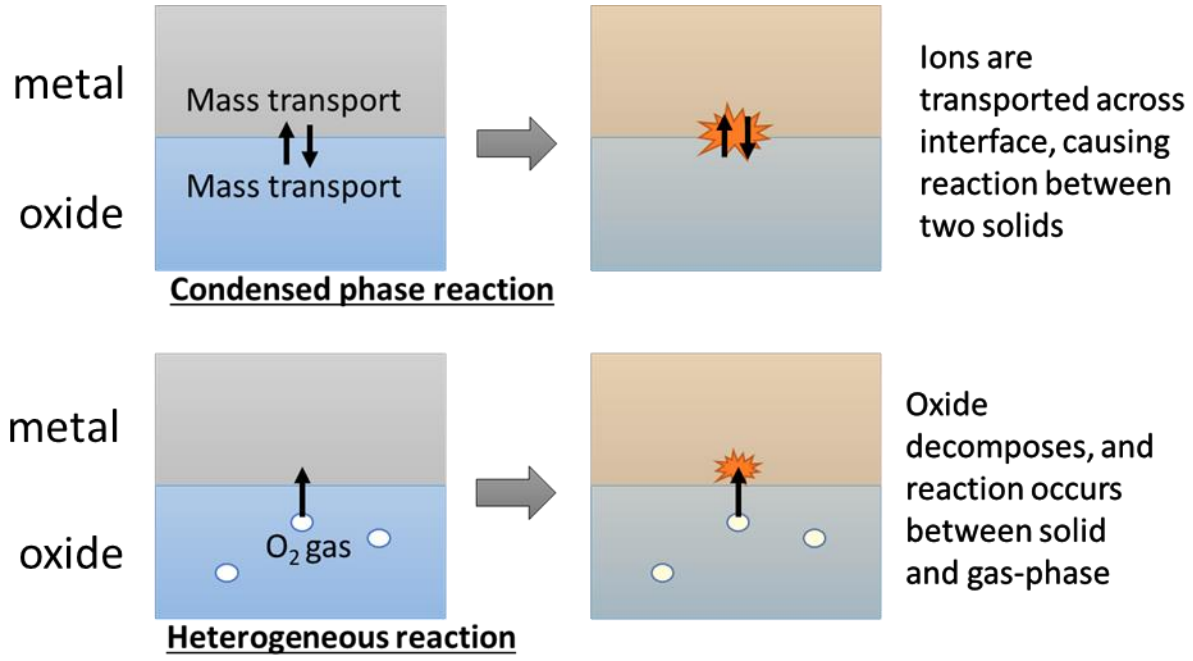

Figure 4-1 Reaction mechanisms for nanothermite materials

Due to the popularity of Al-CuO thermites, from their high heat and gas production (974.1 cal/g and 0.3431 g gas/g reactant, respectively), there is a large body of supporting research in literature (shown in Table 2-2). Among this, the reaction mechanism has been investigated and proposed by a small number of experimental and theoretical models [14] [15] [17]. In contrast, aluminum-cuprous oxide (Al/Cu_2O) thermites have gained much less popularity, and have been the subject of very few studies, especially in terms of the reaction mechanism.

Recently, a study by Abdallah et al. provided an in-depth discussion on the mechanism for Al/CuO reactions [14], and showed that the reaction was initiated by the decomposition of the CuO to Cu_2O and gaseous oxygen, and that the produced oxygen contributed to the oxidation of the Al layer after accumulating at the interface. They also discussed the further reduction of Cu_2O into Cu,

which is a critical intermediate reaction. However, the mechanism of this reduction wasn't discussed in detail and, to my knowledge, no current literature offers a detailed discussion of the mechanism of Al/Cu_2O reactions.

Therefore, it is necessary to gain an understanding of the Al/Cu_2O reaction mechanism for the following reasons. Firstly, it is necessary to understand the reaction mechanism when seeking to understand how structural properties affect the ignition and reaction characteristics. Secondly, due to the lack of supporting literature, there are no current available reaction models to draw information from. With this in mind, this study aims to develop a new method to investigate the reaction mechanism using gas-capture storage and analysis. By utilizing a substrate that becomes sufficiently malleable during the heating process, bubbles of produced gas can be forced into the substrate and stored for analysis. Performing elemental analysis of the bubbles will provide insight on the origin of the gaseous products which will, in turn, provide information on the reaction mechanism. Three possible outcomes of this method will be highlighted in the following discussion. 1) If there is evidence of reaction with no bubble formation or significant mass loss occurring before reaction initiation, this suggests that the reaction took place between solid components, and indicates that a condensed phase reaction mechanism took place. 2) If bubbles formed, and the elemental analysis shows that there is a significant concentration of metal in the bubbles, accompanied by an absence of significant mass loss before reaction initiation, then it can be concluded that the bubbles formed due to rapid metal vaporization caused by the high heat of reaction. 3) If bubbles formed, and the elemental analysis shows an insignificant concentration of metal in the bubbles, accompanied by significant mass-loss before reaction initiation, then it is likely that bubble formation occurred due to the rapid formation of gaseous oxygen. This formation of

gaseous oxygen is caused by the decomposition of the oxide, which would indicate that the samples underwent a heterogeneous reaction mechanism.

4.1 Experimental

Two different structures were produced on glass slides via magnetron sputtering, as shown in Figure 4-2. The first sample had one 135 nm Al layer, and one 220 nm Cu_2O layer, which formed one Al-Cu_2O bilayer. The second sample consisted of two Al-Cu_2O bilayers, with each Al layer approximately 65 nm thick, and each Cu_2O layer approximately 110 nm thick. For both samples, Cu_2O was always the outer layer, and at least one Al layer always shared an interface with the glass substrate. The total thicknesses were 355 nm and 350 nm for the one- and two-bilayer samples, respectively.

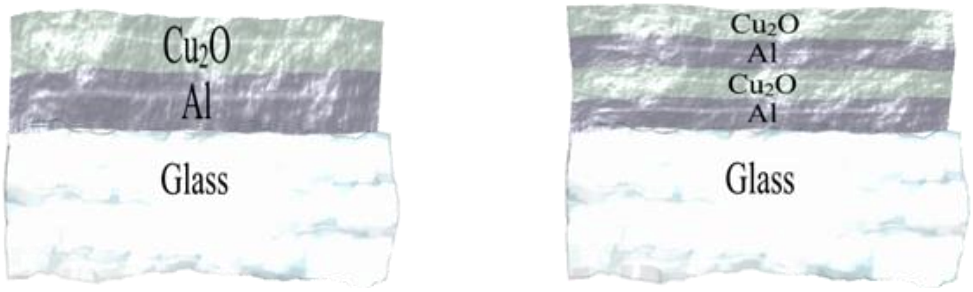

Figure 4-2 Illustration of the (left) one-bilayer and (right) two-bilayer structures deposited on the glass substrate via sputtering

To preserve the characteristics of the structures, and to prevent long-term exposure to oxygen and moisture, as-produced nanolaminates were stored under vacuum until time of use. They were then heated to 800°C in an argon-filled tube oven, and cooled to room temperature. The samples were carefully cut with a diamond knife, and broken so that the cross-section was exposed. Analysis with SEM and EDX was performed to determine the structural characteristics and composition.

DSC and TGA analysis was also carried out to gather information on the reaction and ignition characteristics such as ignition temperature, heat release, and mass loss%.

4.2 Results and Discussion

Figure 4-3 displays SEM images of the one-bilayer (Figure 4-3 a)) and two-bilayer (Figure 4-3 b)) samples after being heated to 800°C in the argon oven. The sample layers can be clearly seen in the one-bilayer sample, with the Cu_2O layer being the top surface, and the darker Al layer forming interfaces with the Cu_2O layer and glass substrate. This image looks identical to the sample before undergoing heating to 800°.

Figure 4-3 b) is an image of the corner of the heated two-bilayer sample, so that both the Cu_2O top surface and substrate cross-section could be observed. Compared to the unheated two-bilayer samples, the heated samples have two major differences. The first difference is the rough, textured appearance on the surface of the Cu_2O layer (shown in the inset of Figure 4-3 b)). This characteristic nanoparticle formation was caused by the vaporization of metals during the thermite reaction (Al and Cu), which then nucleated and grew as the sample cooled, indicating that the reaction temperature has surpassed the boiling point of Al and Cu (2327 °C [56] and 2595 °C [57], respectively) locally. The second major difference is the appearance of bubbles within the substrate. These bubbles are on the scale of microns in diameter, and are distributed along the thermite-substrate interface. They were produced due to the formation and accumulation of gas-phase during the thermite reaction, which was then forced into the malleable substrate and preserved. These bubbles were not observed in any of the samples prior to reaction, and were not observed in the heated one-bilayer samples.

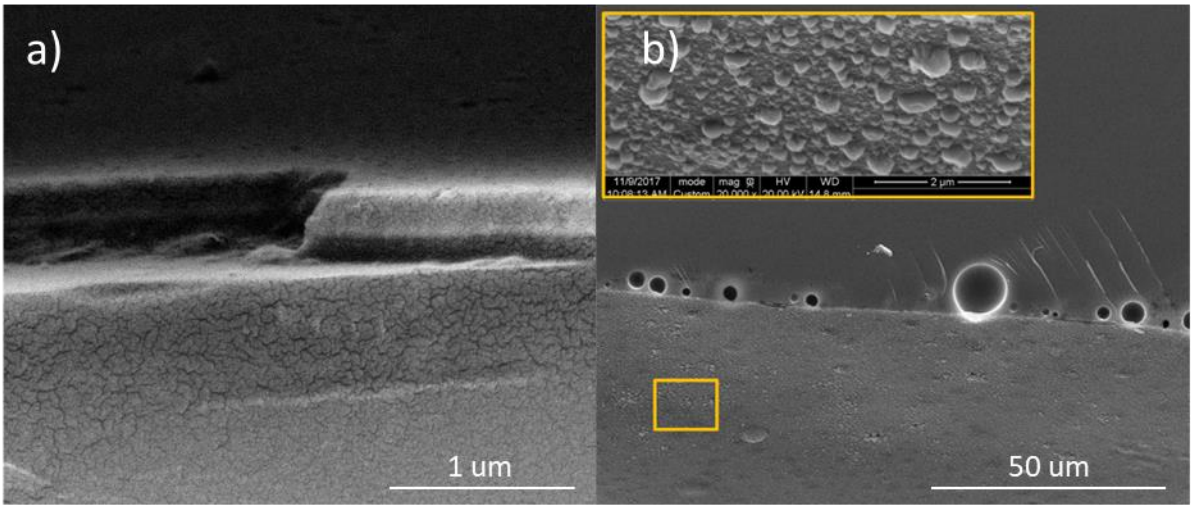

Figure 4-3 SEM images of a) the heated one-bilayer sample and b) the heated two-bilayer sample

To gain insight into the cause of the bubble formation, EDX was used to provide an analysis of the elemental composition. EDX was also used to verify that the original samples contained discrete layers of Al and Cu_2O on glass. Figure 4-4 shows the scan area for EDX analysis of the bubble composition, and also shows the composition results for the area of interest. Aside from background levels (detected in the bulk glass at a similar depth), no significant Al or Cu levels were detected within the bubbles. As mentioned in the Section 4.1, a significant presence of metals within the bubbles would indicate that the bubble formation was due to the vaporization of metals from the high heat of the thermite reaction. However, an insignificant concentration (or absence) of metals signifies that the bubbles were generated by the release of gaseous oxygen during the decomposition of the Cu_2O layer. This is a critical step in the heterogeneous reaction mechanism, since the reaction must occur between the gas-phase oxygen and solid metal fuel.

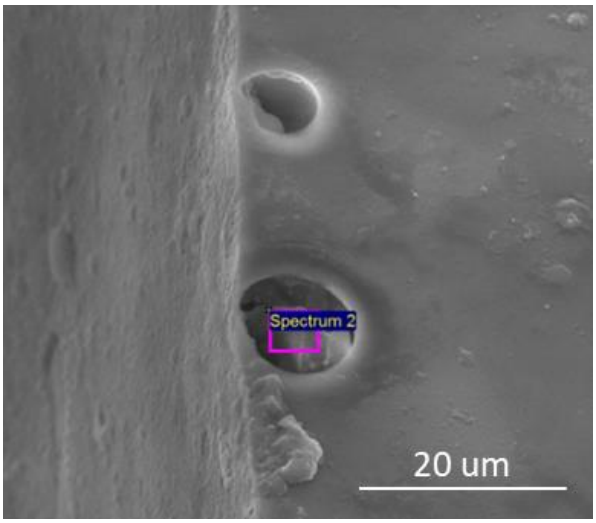

Element	Weight%	Atomic%
O K	55.32	68.41
Al K	3.97	2.91
Si K	40.71	28.68
Totals	100.00	

Figure 4-4 SEM image (left) showing the scan area, and the corresponding EDX composition data (right)

The differences between the heated one-bilayer and two-bilayer samples should also be discussed. The absence of characteristic nanoparticle formation on the surface of the one-bilayer sample, and the absence of bubbles generated along the thermite-substrate interface, indicated that a reaction may not have occurred for the one-bilayer samples. This could be due to the fact that, unlike the two-bilayer sample, there was only a single Cu_2O layer, and that layer was open to atmosphere. During the decomposition of the oxide, the generated gaseous oxygen was released to the surrounding environment before a large enough concentration of oxygen accumulated at the Al-Cu_2O interface to initiate the reaction. In the two-bilayer sample, the inner Cu_2O layer was surrounded on both sides by Al layers, trapping the produced gas within the structure. This shows the limitation of using one-bilayer samples with this method. Using multilayer samples will ensure the most accurate results since the multiple layers will trap gasses within the structure and substrate.

Figure 4-5 shows the DSC (a) and TGA (b) results for the two-bilayer sample during heating in argon to 800°C. The exothermic reaction peak can clearly be observed, starting at 370°C, with the peak minimum at 400°C, for the two-bilayer samples. This range is comparable to what was previously observed in literature for Al-Cu_2O thermites, with a reported peak temperature range of 375-400°C [16]. The heat release is low compared to the theoretical maximum heat release of Al-Cu_2O thermites (2434 J/g [58]), but the theoretical value represents a calculated ideal, and experimental values can't reach this. Comparing to previously reported literature values, the heat release for a structure composed of Al-Cu_2O bilayers (255 nm Al and 745 nm Cu_2O) was ~330 J/g between 350 and 550 ° C [16]. This value is of a comparable magnitude to the heat release obtained for the two-bilayer samples (~200J/g), but the heat release of samples in this study are lower due to the equivalence ratio being further from the ideal stoichiometry. The one-bilayer samples did not show exothermic reaction peaks, further indicating that the exothermic reaction did not occur.

The TGA data, as shown in Figure 4-5 (b) further supports the hypothesis that the Al/Cu_2O nanolaminates follow a heterogeneous pathway during reaction. It can be observed that the slope, representing the rate of mass loss with a constant heating rate, increased at approximately 325°. This indicates that a significant increase in mass-loss occurs prior to the start of the exothermic reaction. This increased mass loss was caused by the loss of oxygen to the environment, due to the decomposition of the oxide, as is characteristic of heterogeneous thermite reactions. Since the mass loss occurs prior to the start of the exothermic reaction (mass loss at 325°C compared to the initiation temperature of 370°C), it indicates that the decomposition of the oxide needed to occur first, further supporting that this is a heterogeneous reaction scheme.

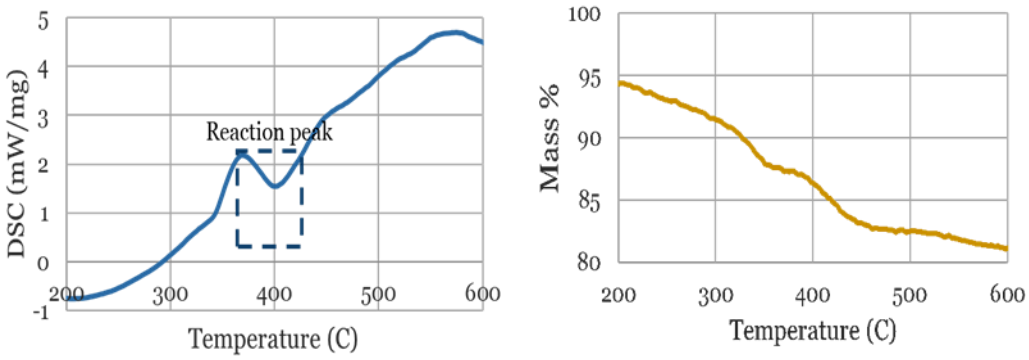

Figure 4-5 the a) DSC and b) TGA results for the two-bilayer sample heated to 800°C in argon

Combining the information from DSC, TGA, SEM, and EDX, the following theoretical reaction mechanism can be outlined (and is illustrated in Figure 4-6) for a multiple-bilayer sample. At room temperature, the structure is stable due to the oxygen being held in the Cu_2O layer. As the temperature is increased, the Cu_2O decomposes to Cu and releases gaseous oxygen. Due to the pressure of the accumulating gaseous oxygen, some of it is forced into the malleable substrate, some escapes to the atmosphere from the surface oxide layer, and some travels to the interface between the Al and Cu_2O layers. Once at the interface, the gaseous oxygen oxidizes the Al, producing Al_2O_3, and heat is produced through this exothermic process. The high heat of reaction vaporizes Al and Cu, which nucleate and form particles on the sample surface as they cool.

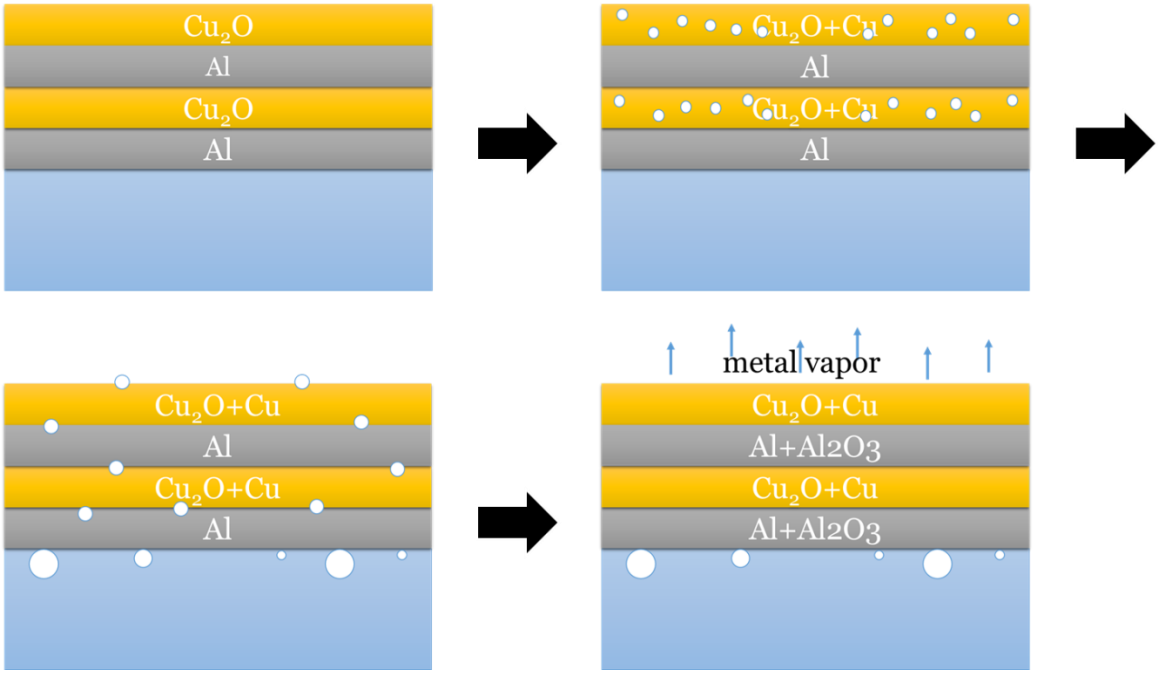

Figure 4-6 Schematic of the proposed reaction mechanism for Al-Cu_2O thermite nanolaminates

4.3 Summary

In this study, a novel method for determining the reaction mechanism of thermite nanolaminates was developed using gas capture and storage. The composition of the produced bubbles indicated that gaseous oxygen was released during the reaction, and TGA data verified that this decomposition occurred prior to the exothermic reaction peak. This indicated that the decomposition of the oxide, to produce gaseous oxygen, was a critical step in the reaction pathway. This is characteristic of heterogeneous reactions, and provided evidence that Al-Cu_2O nanolaminates have a heterogeneous reaction mechanism, contrary to the general belief that nanothermites are dominated by condensed phase reactions [29] [51].

It was also observed that one-bilayer Al/Cu_2O samples do not undergo reaction upon being heated to 800°C. This indicated that there may be a critical amount of gaseous oxygen accumulation necessary to initiate the thermite reaction, which was not reached when the sole oxide layer was

open to the environment. Therefore, one-bilayer samples undergoing a heterogeneous reaction mechanism should not be used with the oxide in an unconstrained (open to atmosphere) state.

5.0 Effect of Structural Characteristics on the Initiation and Reaction Characteristics of Heated Al-Cu_2O Thermite Nanolaminates

When utilizing thermites commercially, as materials for welding and metal refining, it is important to have a reliable, cheap, and efficient ignition source. For welding, it is common to use a sparkler or magnesium ribbon to produce the high heat necessary to initiate the thermite reaction. For metal refining, sparklers, fuses, and heated crucibles and chambers may also be used. Due to this, it is necessary to understand how thermite nanolaminates behave when thermal energy is provided from a heat source.

For this study, a DSC was used to heat the samples at a controlled rate, and record any exothermic or endothermic events that occur. This DSC was coupled with a TGA to provide information on the mass loss events. Using these, information on the initiation temperature, heat release, alloying peaks, and decomposition or vaporization events can be obtained.

By manipulating the structural characteristics of these nanolaminates, and performing the DSC/TGA analysis, conclusions can be drawn regarding the impact that structural factors have on ignition and reaction characteristics. More specifically, varying the layer thickness, the presence of a Cu interlayer, and the type of gas present during reaction will be related to changes in reaction characteristics. Where applicable, these will be related to the reaction mechanism determined in Section 4.0, and will be utilized to provide an understanding of the factors controlling thermite nanolaminate reactions when exposed to heat sources.

A method to improve the stability of thin nanolaminates, utilizing a Cu interlayer, is also introduced in this section. In a 2010 paper by Petrantoni et al. [3], it was shown that Al-CuO thermite nanolaminates become unstable in air below a certain thickness. The thermite reaction

relies on the diffusion and accumulate of oxygen at the metal-oxide interface in order for the reaction to initiate. Therefore, it was theorized that the instability of Al-CuO thermites, with layer thicknesses below 50 nm, was due to the diffusion of oxygen occurring more readily through the ultra-thin layers [3].

5.1 Experimental

The thermite nanolaminates were fabricated using the sputtering method outlined in Section 3.1. The Cu_2O and Al deposition times were varied to examine the effect of changing layer thickness, and a copper layer was added to some samples in order to determine the impact of having a copper interlayer at the Cu_2O and Al interface.

A DSC was used to react the samples and determine the position of any exothermic or endothermic events, and a TGA was used to measure where mass loss events occurred. See section 3.3.2 for information on the DSC and TGA. Since the gas flow in the combined DSC/TGA device could be controlled, experiments were carried out under both argon flow and air flow to determine if the presence of environmental oxygen would impact the reaction.

XPS analysis of the Cu_2O layer was also carried out in order to gain an understanding of the oxide composition and see if the surface composition of the oxide differs from the bulk composition. The NIST XPS database was used to match the peak positions to the materials present in the sample. Please refer to Section 3.3.3 for more information on the XPS device.

5.2 Results and Discussion

Figure 5-1 shows SEM images of the thermite nanolaminate sample before and after reaction. The unreacted samples are shown in a) and b), and c) and d) show the samples after being heated to 800°C in DSC. The unreacted samples have a rolled hollow-cylinder morphology caused by the

fabrication process. Making up the cylinders are multiple Al, Cu_2O, and sometimes Cu layers ranging from 5nm-300nm in size (sample dependent). For the reacted samples, the surface of the cylinders have gained a textured appearance due to characteristic nanoparticle formation during reaction. The high heat production causes the vaporization of metals (Al and Cu), which nucleate and form particles on the sample surfaces as it cools. These nanoparticles are present in all the SEM images of reacted samples. It should also be noted that the structures in these images have maintained their structural integrity and hollow-cylinder shape. This indicates that the heat produced during reaction did not surpass the melt temperature of Al_2O_3 and Cu_2O, which allows the structure to maintain it's original morphology. For structures with heats of reaction that surpass the melt temperature of Al_2O_3 and Cu_2O, the cylinder morphology is not maintained, and the samples gain a melted appearance.

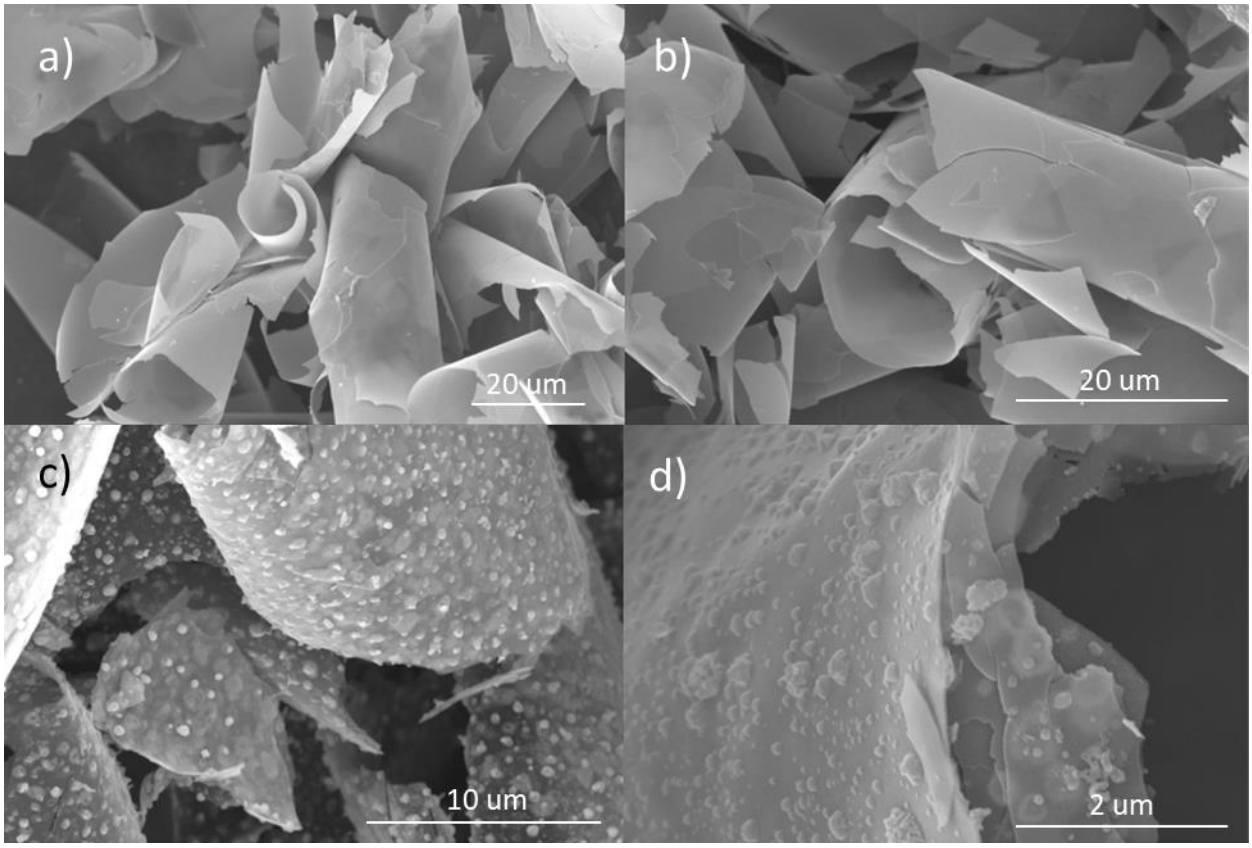

Figure 5-1 SEM images of (a) and (b) typical unreacted samples, (c) a reacted sample, and (d) nanoparticles on the surface of a reacted sample

When performing DSC and TGA tests, argon is often used as the gas of choice since it provides an inert atmosphere during reaction. However, it was determined that the chosen gas flow had an affect on the reaction data. Figure 5-2 shows the TGA and DSC data for samples reacted in a) argon and b) air, and three main differences were observed. The first difference is that the energy release (area of the exothermic peak) was larger for the samples reacted in air. In this case, the samples being tested were oxygen deficient due to having a Cu_2O layer thickness below what is stoichiometrically required. Therefore, oxygen from the environment was utilized in the reaction, leading to a higher energy release. The second difference was the shape of the TGA curve. For samples reacted in argon, there were two mass-loss events (starting at ~310 °C and ~385 °C),

marked by dotted lines on Figure 5-2 a). The first mass-loss event occurred prior to the exothermic reaction peak (starting at ~370 °C), and signified the decomposition of the oxide layer (and release of gaseous oxygen) that occurs for heterogeneous reactions. The second mass-loss event occurred after the initiation of the exothermic event, and is due to mass loss from metal vaporization. For the samples reacted in air (Figure 5-2 b)), only one strong mass loss event was observed (marked by the dotted line at ~280 °C), and this event occurred during the exothermic reaction (starting at ~275 °C). This could indicate that, because of the presence of environmental oxygen, and the nanoscale thickness of the nanolaminate layers, environmental oxygen was able to diffuse through the layers and initiate the thermite reaction prior to the decomposition of the oxide. This was further supported by the shifting of the reaction initiation to lower temperatures, which was the third difference between the two data sets. For samples reacted in argon, the reaction initiated at ~370 °C, whereas the initiation temperature drops to ~275 °C when reacted in air. In argon, the decomposition of the oxide occurred at ~310 °C, which is why this mass loss event is missing from the TGA data for the sample reacted in air. This shows the importance of considering the reaction medium when designing thermite nanolaminates.

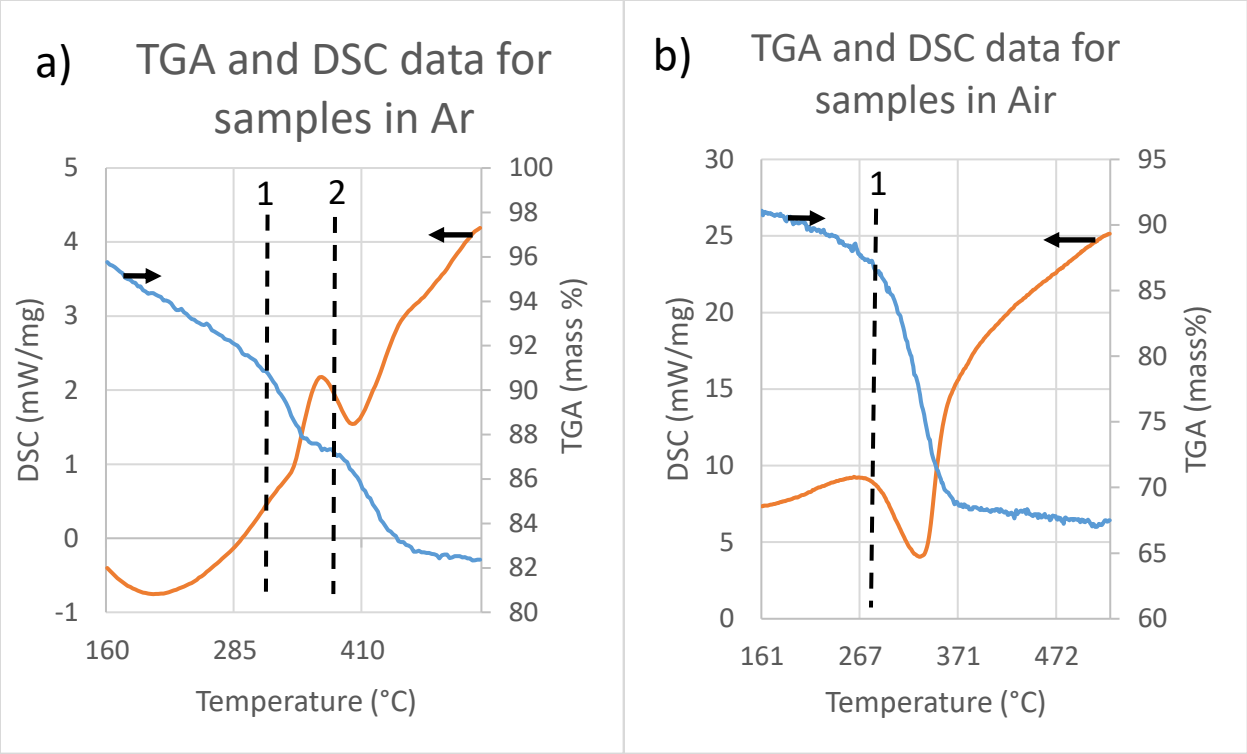

Figure 5-2 DSC and TGA data for samples reacted in a) argon flow and b) air.

To examine the effects of the Cu_2O layer thickness on the reaction and initiation characteristics, thermite structures with different layer thicknesses were fabricated and tested with DSC under argon flow. Figure 5-3 shows the DSC data comparison between three samples with an Al thickness of ~40 nm, and Cu_2O layer thicknesses of ~45 nm, ~75 nm, and ~90 nm. On the Figure, dotted lines are used to mark the beginning of the exothermic events, and are color coded to represent each sample. From this, it was observed that the ~45 nm Cu_2O sample had the lowest initiation temperature (~350 °C), whereas the ~90 nm sample had the highest initiation temperature (~380 °C). This observed phenomenon can be related to the reaction mechanism determined in Section 4.0. As this is a heterogeneous reaction mechanism, a critical step involves the decomposition of the oxide to release gaseous oxygen, which accumulates at the Al-Cu_2O interface

and oxidizes the Al. Reducing the size of the Cu_2O layers resulted in a decreased diffusion distance for the gaseous oxygen, which allowed the reaction to occur at a lower temperature. The size of the exothermic peak, which signifies the energy release during the exothermic event, varied between these samples. This can be explained by the differences in stoichiometry, where certain Al:Cu_2O ratios were more ideal.

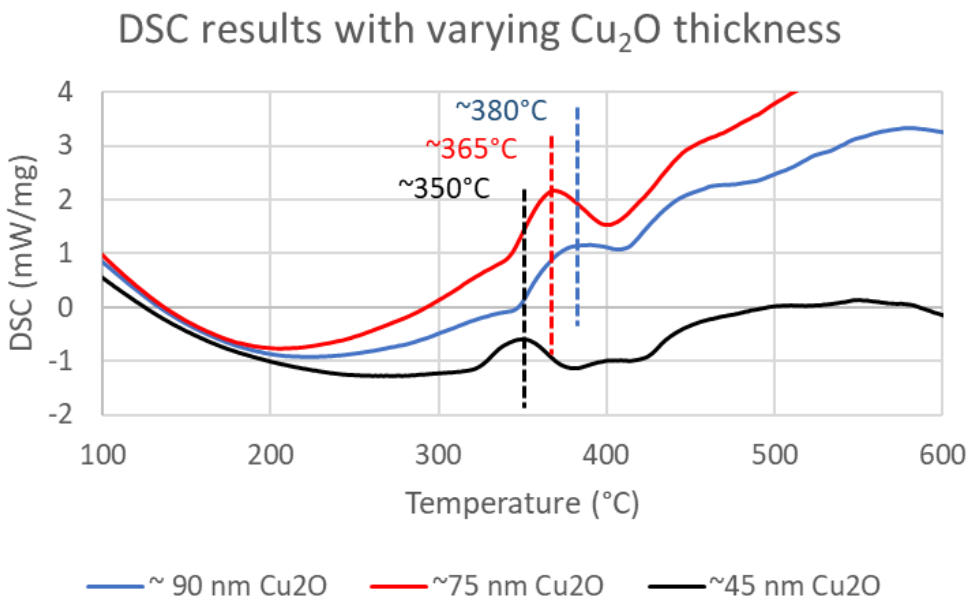

Figure 5-3 DSC results showing the effect of varying the Cu_2O thickness

Figure 5-4 displays an SEM image of a sample that had copper interlayers incorporated between the Al and Cu_2O layers. These structures had Cu_2O as the outermost layers, Al as the innermost layer(s), and pure Cu between the Cu_2O and Al layers. This particular sample had 5 total layers, but the layer thicknesses, and total number of layers, was varied for different structures. In the structure shown in Figure 5-4, the Cu_2O layers had a thickness of 226.5 +- 13.5 nm, the Cu layers had a thickness of 137.9 +- 4.5 nm, and the Al layer was 73 nm.

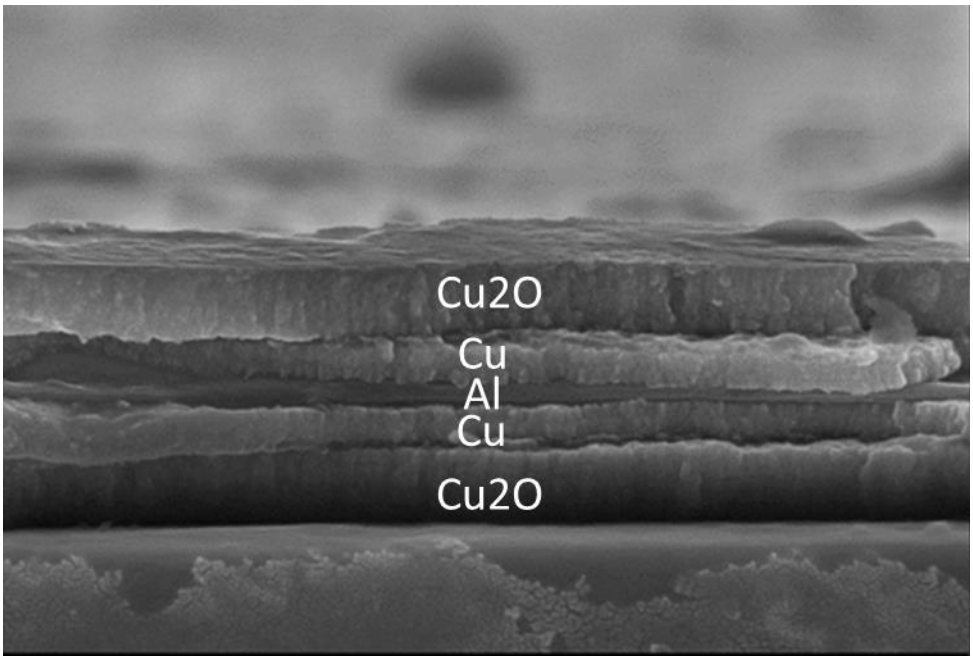

Figure 5-4 SEM image showing the symmetric layered structure of the thermite nanolaminates

The DSC data comparing structures with and without the Cu interlayer is shown in Figure 5-5. For these structures, the Al layer has a thickness of ~25 nm, the Cu_2O layer had a thickness of ~30 nm, and the optional Cu interlayer had a thickness of ~15 nm. The exothermic reaction peak for the sample with the Cu interlayer is clearly marked in Figure 5-5 a). However, for the sample without the Cu interlayer, no reaction peak is observed. This indicates that the Cu interlayer was able to impart increased stability to the structure, allowing it to maintain it's reactivity. In contrast, the sample without the interlayer reacted prior to DSC measurement. A paper by Petrantoni et al. [3] previously reported on the spontaneous ignition of Al-CuO nanolaminates when the layer thicknesses were reduced below 50 nm, and attributed this to a decrease in stability caused by an inability to prevent oxygen diffusion from atmosphere. Given the improvement in stability caused

by the addition of a Cu interlayer, it is hypothesized that the Cu layer act as a barrier to oxygen diffusion. In this case, the Cu barrier ensures that a sufficient concentration of environmental oxygen is unable to collect at the Al-Cu_2O interface to trigger the exothermic reaction. Another point of interest is the slight exothermic peak indicated in Figure 5-5 b). This slight exothermic peak is only observed in samples with the Cu interlayer, and has been attributed to the alloying of Al and Cu metals [21]. Both $CuAl_2$ and Cu_9Al_4 are suggested alloys [21].

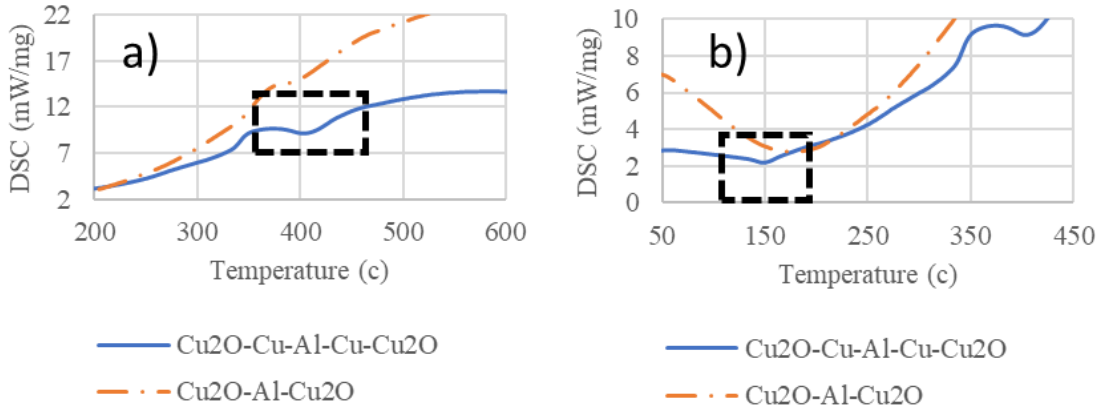

Figure 5-5 DSC plots showing the a) exothermic reaction peak and b) low-temperature Cu-Al alloying peak

Although the addition of a Cu interlayer was shown to increase the stability of sufficiently thin nanolaminate structures, another important feature of adding a copper interlayer is that it lowers the ignition temperature. This is due to the fact that there is a strong drive for Cu diffusion into Al, and heating to 150°C results in a significant amount of Cu incorporation into the Al layer [21]. This results in Al-Cu alloy formation in the bulk, and removes the barrier to oxygen diffusion during heating. As shown in Figure 5-6, the exothermic peak for a sample (40 nm Al thickness and 45 nm

Cu_2O thickness) with an ~8 nm copper interlayer occurs at a lower temperature than the exothermic peak for a sample without a copper interlayer. The initiation temperature is roughly 279°C for the sample without the copper interlayer, and 265°C for the sample with the copper interlayer. This effect was previously shown in literature, and this enhancement of reactivity was attributed to alloying between Al and Cu, which was able to decrease the metallic melting temperature of Al and increase the reaction propagation velocity [21]. It should be noted that the DSC data in Figure 5-6 differs from that of Figure 5-5. This is again attributed to the differences in the reaction environment, where the samples in Figure 5-6 and Figure 5-5 were reacted in air and argon, respectively. As discussed, environmental oxygen can contribute to the thermite reaction, resulting in an earlier onset temperature and a more-exothermic reaction.

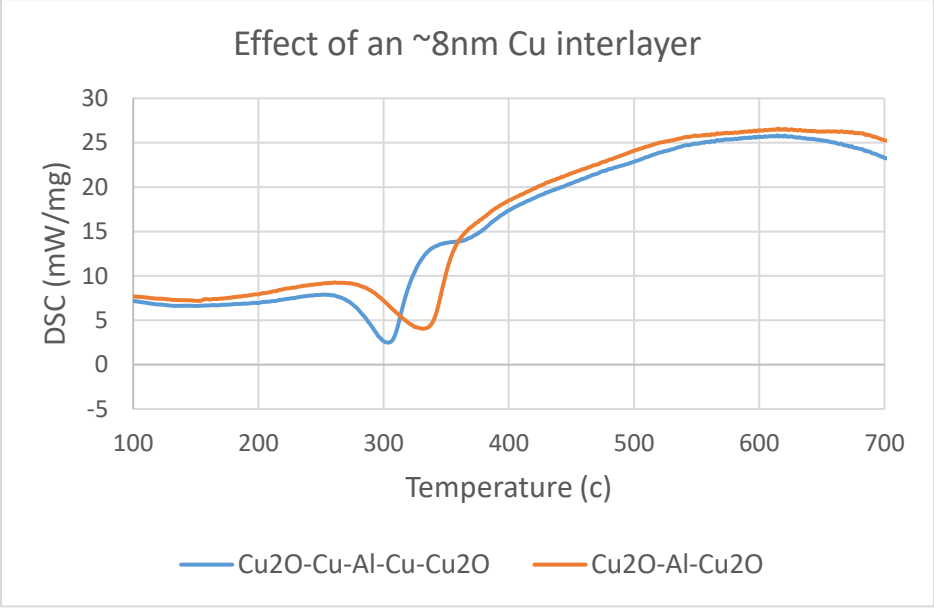

Figure 5-6 Comparison of the exothermic reaction peaks for samples reacted in air with and without a Cu interlayer (Al ~40 nm, Cu_2O ~45 nm, Cu ~8 nm)

A comparison of the TGA data for two different structures reacted in air is shown in Figure 5-7. Both structures have Cu_2O layers of approximately 45 nm in thickness, and Al layers of approximately 40 nm in thickness. Only one of the structures has a Cu interlayer of approximately 8 nm in thickness, and is labelled as "Cu_2O-Cu-Al-Cu-Cu_2O". It can be observed that the major mass-loss event (occurring at ~300°C) is larger for the sample without the Cu interlayer. More specifically, the sample without the Cu interlayer loses 10.8 mass% between 300 and 400°C, whereas the sample with the Cu interlayer only loses 5.14 mass%. This mass loss is attributed to ability of Cu interlayers to reduce the gas generation during reaction, as was previously observed in a Paper by Kinsey et al. [16].

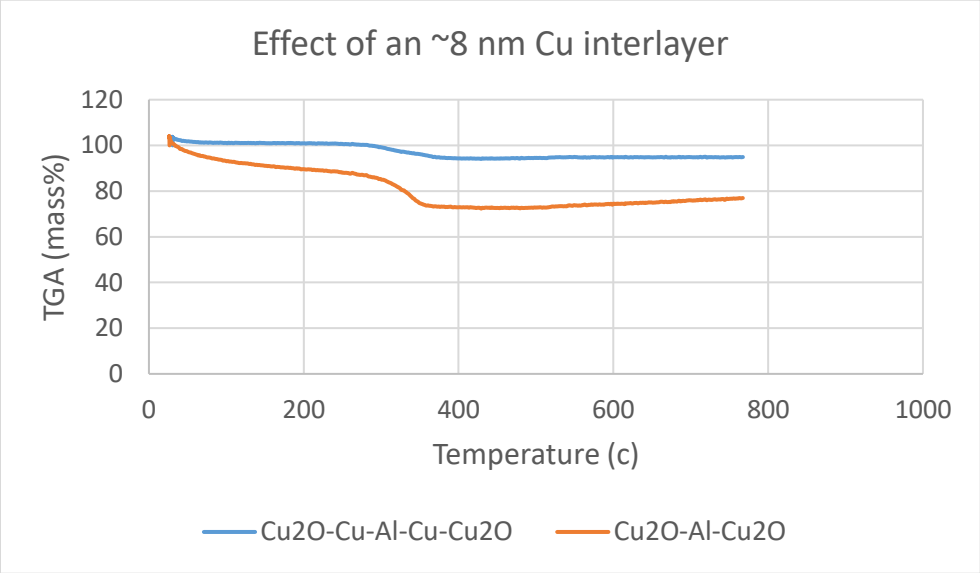

Figure 5-7 Comparison of the TGA data for samples reacted in air with and without a Cu interlayer (Al ~40 nm, CuO ~45 nm, Cu ~8 nm)

Figure 5-8 shows the XPS data for the (a) sample surface and (b) sample bulk. The surface measurements were taken directly of the sample surface, and then focussed ion beam (FIB) was used, in vacuum, to remove the top layers of material. This was done to gain an accurate profile of the material composition, and to understand whether the surface material differs from the bulk. It can be observed that the XPS signal for the surface varies from the XPS signal of the bulk. For the surface, the 2P1/2 peak is at 953.7 eV, the 2P3/2 peak is at 933.4 eV, and a 2P3/2 satellite peak is at 943 eV. Comparing this to the values in the NIST XPS database, it was determined that the surface was composed of a thin layer of CuO. For the bulk material, the 2P1/2 peak was at 952.3 eV, the 2P3/2 peak occurred at 932.5 eV, and a very weak satellite peak occurred between the other two peaks, indicaxting that the bulk is composed of Cu_2O. See Appendix B for a Figure representing the differences in the CuO and Cu_2O binding energy plots. This suggests that the Cu_2O oxide layer will interact with environmental oxygen over time, and change to CuO oxide. Since the formation of CuO requires that it be exposed to oxygen from its environment, CuO will only form on the outside of the nanolaminate structure, and will not affect any of the Al-Cu_2O interfaces. Therefore, this CuO layer plays an insignificant role in the thermite reaction for these samples

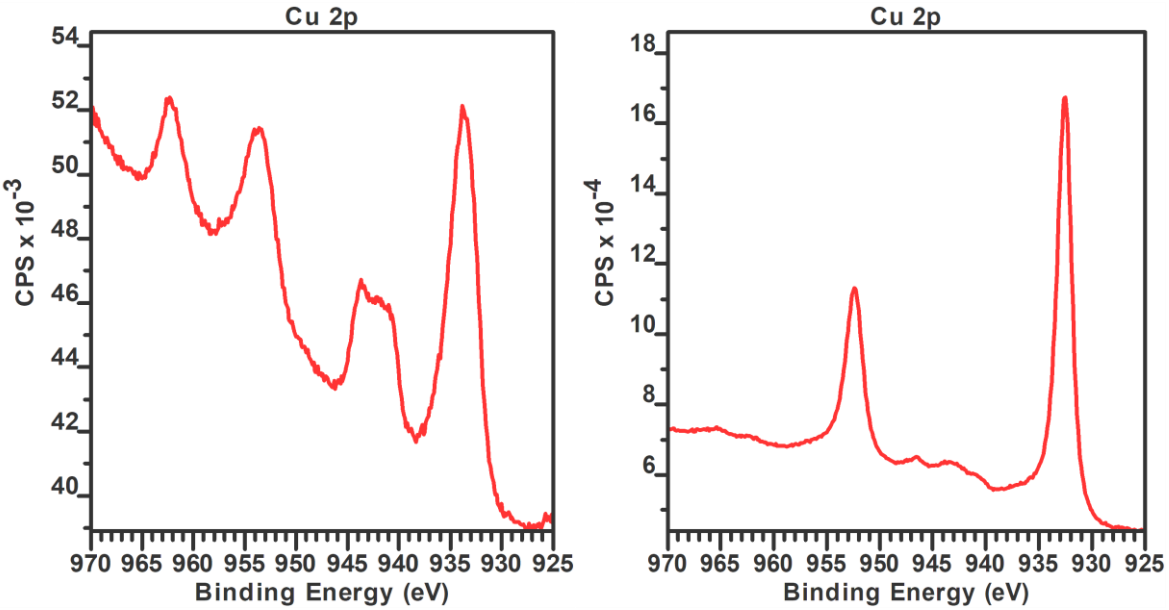

Figure 5-8 XPS results of the (a) sample surface and (b) sample bulk after FIB removal of the surface layer

5.3 Summary

In this study, the effects of layer thickness, presence of a Cu interlayer, and the choice of reaction gas on the initiation and reaction characteristics was examined. A summary of the properties, variables, and mechanisms by which they are affected is given in Table 5-1.

Table 5-1: Summary of the properties, variables affected, and the mechanisms by which they are affected during heating in DSC

PROPERTY	AFFECTED VARIABLE	MECHANISM
Cu_2O layer thickness	initiation temperature	oxygen diffusion
	energy release	ratio of components
Al layer thickness	energy release	ratio of components
Cu interlayer	initiation temperature	alloy formation
	energy release	reduction in active material
	stability	barrier to oxygen diffusion
choice of gas for reaction environment	energy release	utilization of environmental oxygen in reaction
	initiation temperature	diffusion of environmental oxygen into structure

Varying the Cu_2O layer thickness showed an effect on the initiation temperature of the thermite reaction. This can be attributed to the effect that layer thickness has on the diffusion of oxygen, and the effect of layer thickness on melting temperature.

The energy release can be tailored by varying the thickness of the Cu_2O and Al layers relative to one another. Energy release will be most favorable when the thicknesses of the reactant layers approach the ratio for ideal stoichiometry.

The introduction of a Cu interlayer between the Al and Cu_2O layers was shown to improve the stability of sufficiently thin nanolaminates by acting as a barrier to oxygen diffusion. It also displayed the positive effect of lowering the initiation temperature through the formation of Al:Cu alloys, which lowered the metallic melting temperature of Al [21]. However, caution should be used

when incorporating Cu interlayers since it could impact the energy release by reducing the overall amount of active material per mass of sample.

Finally, the gas present in the reaction environment has shown to be a consideration in the reaction properties of thermite nanolaminates. In the case of samples that are deficient in oxygen (ie: the oxide thickness is not sufficiently large, in comparison to the Al thickness, to provide enough oxygen for a complete reaction), environmental oxygen can be incorporated. This causes an increase in the energy release, and could also result in enhanced flame propagation rates. The presence of environmental oxygen during reaction was also shown to decrease the ignition temperature for the thermite nanolaminates. This was attributed to the fact that Al-Cu_2O undergoes a heterogeneous reaction mechanism, and requires the oxide to decompose and produce gaseous oxygen. In an environment where gaseous oxygen is available, the thermite reaction can occur prior to the decomposition of the oxide.

6.0 Effects of Structural Characteristics on the Laser Ignition of Al-Cu_2O Thermite Nanolaminates

Developments in thermite technology has led to them becoming attractive materials for micropropulsion, microwelding, and MEMs devices. Their application for MEMS has gathered significant interest, and there is a growing body of research supporting their use as micro-actuators, initiators, spot-heaters, and for the generation of pressure pulses.

Due to the small size of MEMs devices, and the sensitivity of device components, laser illumination becomes an appealing ignition source. The tunability of laser power densities and spot sizes (through focussing) makes them able to deliver accurate doses of energy to specific areas of MEMs devices. This allows them to specifically target and initiate the thermite reaction without heating the entire MEMs device. Unlike conductive heating methods, laser ignition does not require a heat source to be in contact with the device, which protects delicate components. Finally, lasers offer a wide variety of specific wavelengths or wavelength ranges, allowing for the laser selection to be optimized for each application.

Given the clear advantages of laser ignition for MEMS devices incorporating thermite materials, this study aims to gain an understanding of how manipulating the structural characteristics of thermite nanolaminates effects the reaction and ignition characteristics. More specifically, this study aims to understand how the ignition delay, initial energy transfer rate (flame spread), and average energy release are affected by oxide thickness, metal thickness, and the presence of a copper interlayer.

6.1 Experimental

The experimental set-up for laser ignition testing is shown below in Figure 6-1. A diode laser (808nm, 2.97 W, 0.2 mm x 1.8 mm FWHM spot size) was used as the ignition source, and the pulse duration was set as 200ms. A high-speed camera (Photron Fastcam SA1.1) was used to capture the ignition and reaction, with a speed of 100000 fps, and a photodiode (Osram SFH206K) was used to capture the light intensity. For each test, the sample was loaded into the metal sample holder (3mm diameter). External software was used to trigger the diode laser and camera simultaneously, and a mirror focussed the laser beam onto the sample surface.

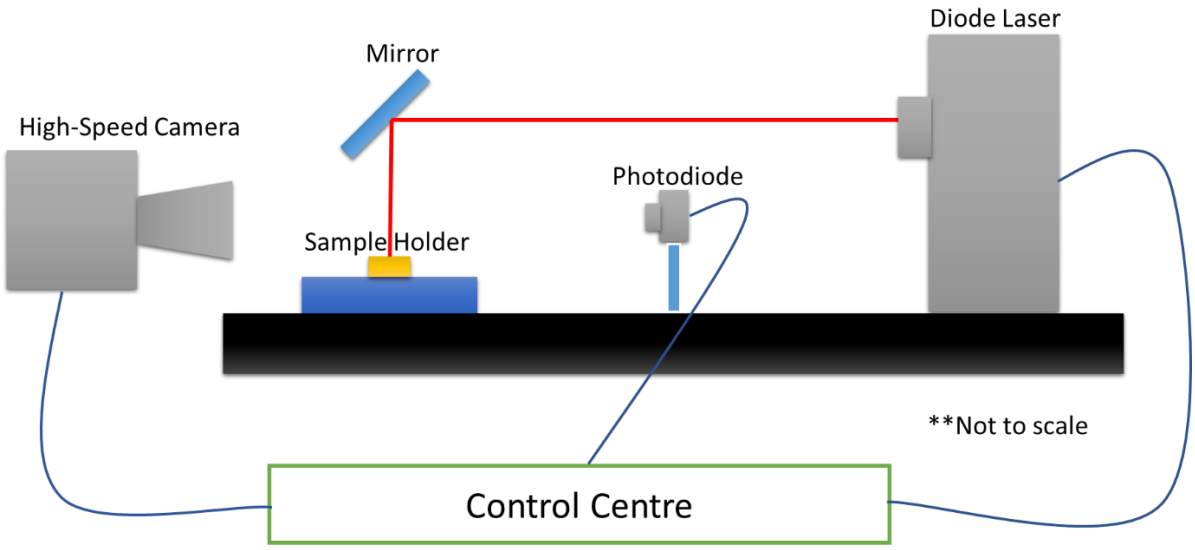

Figure 6-1 Schematic of laser ignition set-up

After illumination and ignition, the ignition delay was measured from the photodiode signal. As shown in Figure 6-2, the initial "jump" in the photodiode signal indicates the beginning of laser illumination, and the second "jump" in the photodiode signal indicates the beginning of the thermite reaction. The linear portion, between the beginning of the laser illumination and the

reaction initiation, gives the ignition delay. This delay can also be verified via high-speed camera by finding the difference between the timestamps of the frames where laser illumination begins and where ignition begins. Both these values were comparable for all samples.

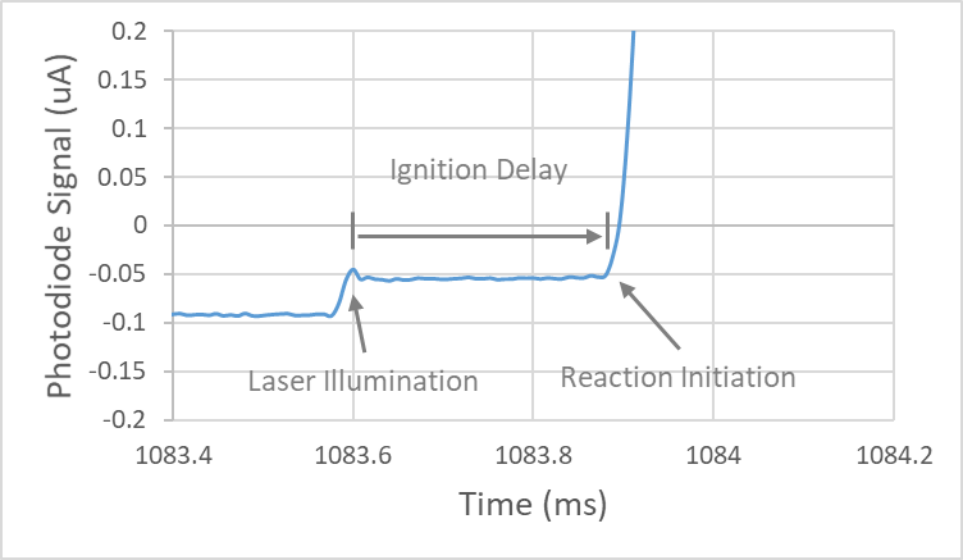

Figure 6-2 Determining the ignition delay of thermite nanolaminates using photodiode data

The rate of expansion of the flame plume was found by analyzing the high-speed camera data. For this, the area of saturated pixels was determined at 10 µs intervals in the reaction video. This rate of increase of the saturated area represents the rate of the flame expansion, and represents the initial energy transfer rate of the samples undergoing reaction. Photos showing this process are given in Figure 6-3.

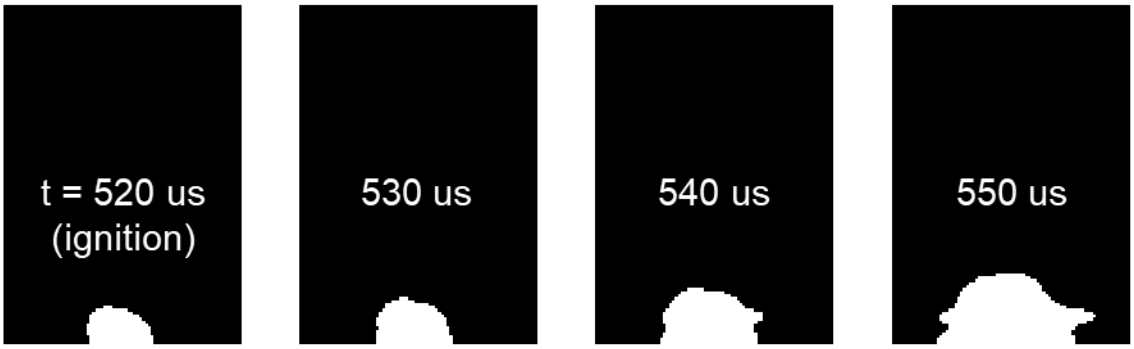

Figure 6-3 Determining the rate of flame expansion. From [59]

To determine the average energy release rate of the samples, the photodiode signal was integrated with respect to time, and normalized by the sample mass. Finally, SEM images were taken of the reactants and products.

6.2 Results and Discussion

The ignition delays were calculated for each sample, and plotted to show the change in ignition delay with varying Cu_2O thickness (with constant Al thickness of 45 nm) or varying Al thickness (with constant Cu_2O thickness of 54 nm). See appendix C for a description of the samples used. These results are shown in Figure 6-4. It can be observed that varying the Al thickness has little impact on the ignition delay, as indicated by the relatively linear trend of the Al-varying trace. However, a U-shaped curve was observed when varying the Cu_2O thickness, leading to a point of minimum ignition delay (at ~50-70nm thickness). This finding is significant because it indicates that varying the Cu_2O thickness can have a substantial impact on the ignition delay of thermite nanolaminates, and that changing the Al thickness has almost no impact.

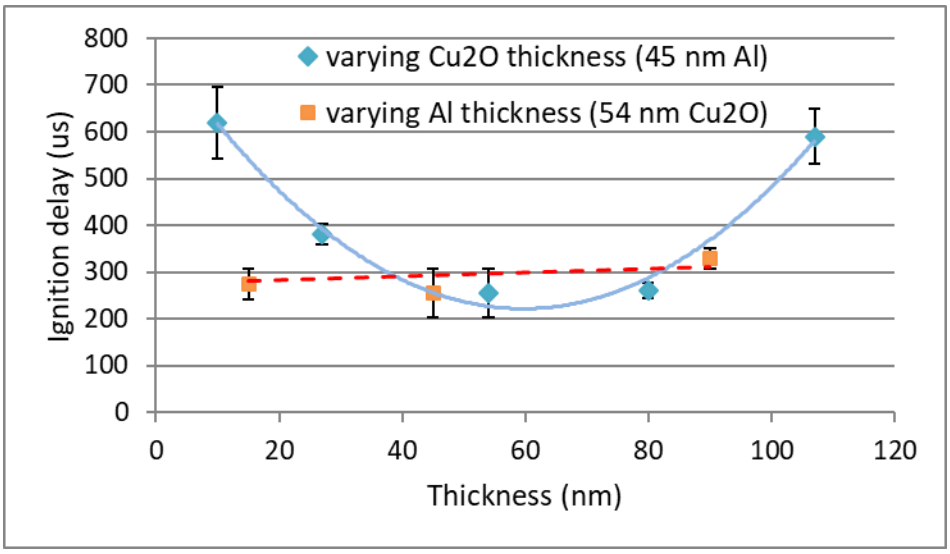

Figure 6-4 The effect of varying the layer thickness on the ignition delay. From [59]

Given that the Cu_2O thickness is the controlling factor for tuning the ignition delay, and that it displays fundamentally different behaviour compared to Al, the mechanism with which this occurs should be considered. It is postulated that this Cu_2O behaviour is due to two competing phenomena: laser absorption and mass diffusion, which will be introduced in the following two paragraphs.

To explain the influence of mass transport, the reaction mechanism determined in Section 4.0 will be referenced. It determined that Al/Cu_2O thermites undergo a heterogeneous reaction pathway where the decomposition of the oxide, to produce gaseous oxygen, is a critical step. The exothermic reaction then begins once the gaseous oxygen has moved to the interface and starts to oxidize the Al. Therefore, the mass diffusion of gaseous oxygen through the Cu_2O layer is a rate-limiting step. This could explain why the ignition delay for the samples increases as the Cu_2O layer thicknesses increase above 80 nm, since increasing the layer thickness increases the distance over which mass diffusion must occur and, therefore, increases the time needed for ignition. This also

explains why the Al layer thickness seemed to have minimal effect on the ignition delay. Considering that the exothermic reaction depends on the decomposition of the oxide, and is rate-limited by the mass transport of gaseous oxygen, varying the Al thickness will have no affect on the decomposition and mass transport of oxygen.

To explain the effect of laser absorption, the reaction mechanism determined in Section 4.0 will again be referenced. This heterogeneous reaction mechanism requires decomposition of the oxide, to produce gaseous oxygen, before the exothermic reaction can begin. For decomposition to occur, the oxide needs to gain a sufficient amount of thermal energy and, as this thermal energy is being provided by laser illumination, the amount of absorbed power will determine how quickly the required thermal energy is reached. This could explain why the ignition delay increases as the thickness of the Cu_2O layers are reduced below ~40 nm, since reducing the layer thickness reduces the amount of power absorbed in the Cu_2O surface layer. Therefore, longer laser illumination is required before a sufficient amount of thermal energy is obtained.

To further understand the role of laser absorption in thermite ignition delays, Lumerical software was used to create a plot of the power absorption per volume (in reference to the original power) versus the Cu_2O thickness. To do so, a 2D multilayered structure of Al and Cu_2O was modelled in the software, and the built-in materials database was used for the refractive index and extinction coefficients. Figure 6-5 shows the simulation set-up, where the laser source is defined so that it hit the surface of the sample and penetrates into the layers.

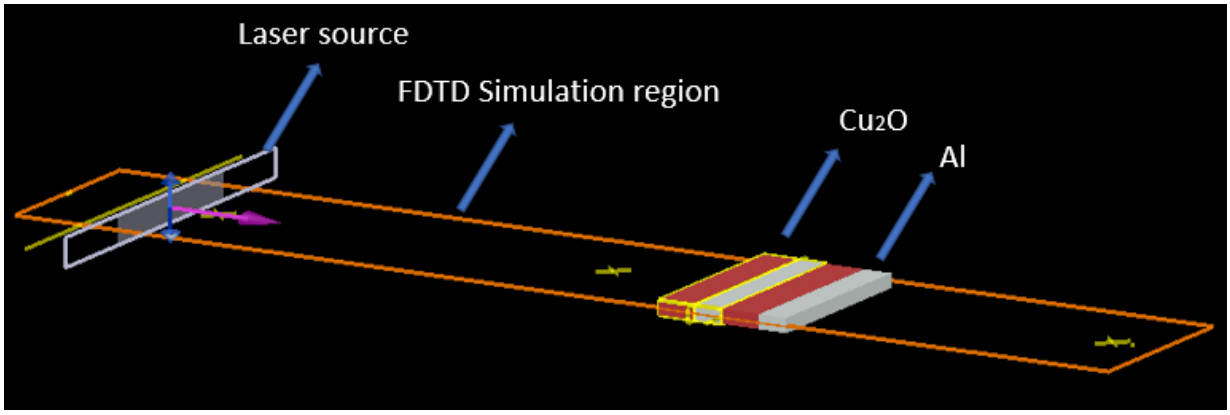

Figure 6-5 Simulation of laser absorption in the thermite nanolaminates

The power absorption per unit volume was calculated following Lumerical's method. This method relies on the use of a finite-difference time-domain (FDTD) method to determine the imaginary part of the permittivity and the electric field intensity, which can be used to calculate the absorbed power (P_{abs}) as shown in equation (3) [60].

$$P_{abs} = -0.5|E|^2 imag(\varepsilon) \tag{14}$$

For general FDTD modeling methods, the material regions and parameters (such as permeability, permittivity, and conductivity) are defined at the start. The FDTD method follows a leap-frog progression where the electric and magnetic fields are solved in sequential moments in time [61]. These values are then advanced in time, and each updated value is dependant on the previously stored values. For a more detailed explanation on the implementation and derivation of FDTD methods, please see the online material provided by J. Schneider [61].

Examining the Power absorption results, as shown in Figure 6-6, it can be observed that there is an increase in power absorption that peaks for a Cu_2O thickness of around 42 nm. This shows a similar trend to what was observed experimentally, where the lowest ignition delays occurred at Cu_2O thicknesses of approximately 50-70 nm. It makes sense that the maximum power absorption should correlate to the minimum ignition delay, since maximum power absorption should cause the layer to reach the ignition temperature most quickly. However, the slight shift between the points of maximum power absorption and minimum ignition delay can be explained by the following: 1) The properties of the sputtered Cu_2O, such as roughness, uniformity, etc., differ from the idealized properties of Cu_2O in the built-in Lumerical database. Therefore, the built-in refractive index utilized by the Lumerical software may differ from the refractive index of the sputtered layers. 2) The model does not take into account the presence of the Al_2O_3 region and intermixed regions at the interface, caused by the energetic sputtering process, which could influence the real-life absorption and transmission. 3) The model does not take into account the thin surface layer of CuO that form on the Cu_2O surface when exposed to environmental oxygen, which was found by XPS analysis discussed in Section 5.0.

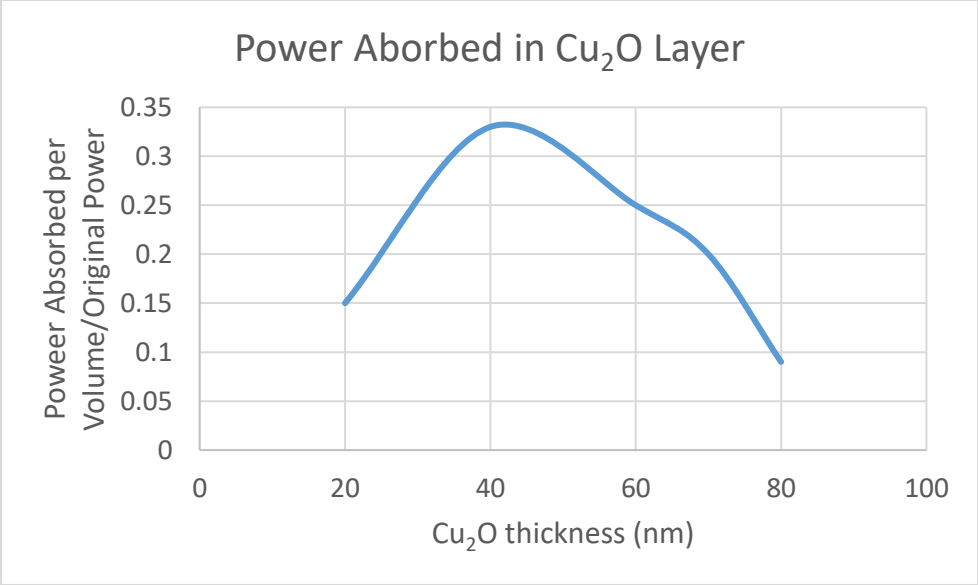

Figure 6-6 Plot of the calculated power absorbed within the Cu_2O layer

Although the experimental and modelled results have a slight shift between the point of maximum power absorption and the point of minimum ignition temperature, the overall shape and trend are similar. This strongly indicates that the trend noticed for ignition delay is largely influenced by the laser absorption of the Cu_2O layers. This also suggests that the effect of mass transport on the ignition delay may not be significant at these length scales. All of the samples tested had Cu_2O layers of <110 nm and Al layers of 45 nm, allowing the laser to penetrate to the interface between the active materials. The heating of the interface, coupled with the nanoscale distances for mass transport, result in a mass transport being a less significant factor in tuning the ignition delay. It should be noted, however, that mass transport plays a significant role when the sample layers are increased to the microscale [59].

Figure 6-7 shows the average photodiode signal and rate of flame expansion for varying Cu_2O layers with a constant 45 nm Al thickness. It can be observed that, as the thickness of the Cu_2O layers increase, the rate of flame area expansion also increases. This is due to the fact that these

structures are approaching the optimal equivalence ratio to enhance the rate of flame expansion. Similarly, the averaged photodiode signal, indicating the energy release, also increases as the Cu_2O layer thickness is increased. This is due to the sample stoichiometry approaching the stoichiometry for optimal heat release, which occurs at an equivalence ratio of 1. For these samples, the equivalence ratios were approximately 16, 6, and 3 for the samples with Cu_2O layers of 10 nm, 27 nm, and 54 nm, respectively. As mentioned in Section 2.2, for a complete reaction, the ratio of Cu_2O to Al by weight is approximately 8:1.

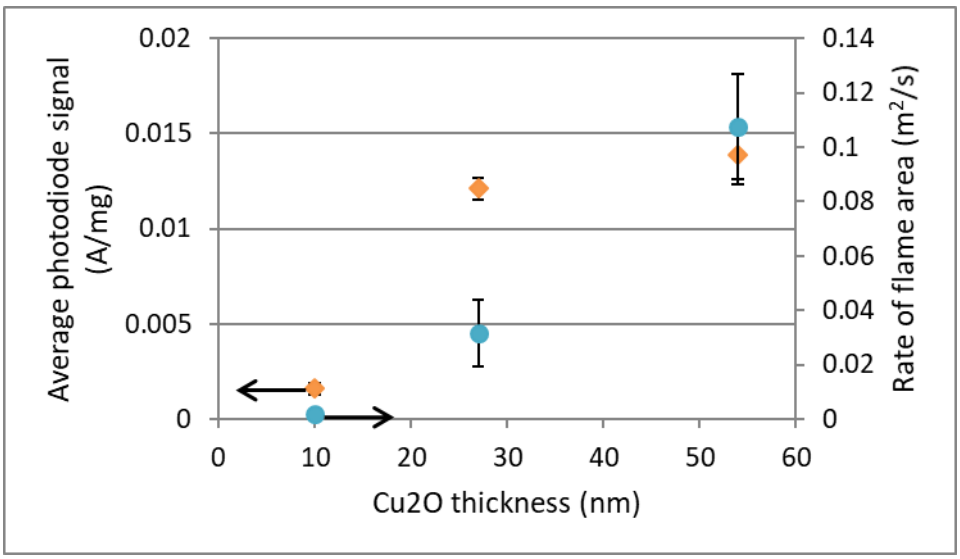

Figure 6-7 effect of varying the Cu_2O layer thickness on the energy release and rate of flame expansion. From [59]

Figure 6-8 a) shows an SEM image of the thermite nanolaminates before reaction. During the removal process, the thin layered structures come off the substrate in flakes (due to the dissolving photoresist), and roll into themselves due to surface forces. These produce hollow cylinders and flakes of layered material, and the inset of Figure 6-8 a) demonstrates the typical layered

appearance of the cross-section of one of the flakes. Figure 6-8 b) and c) show SEM images of two reacted samples with 27 nm Cu_2O layers and 54 nm Cu_2O layers, respectively. For both samples, the Al layers were kept constant at 45 nm. For the reacted 27 nm-Cu_2O samples, the nanolaminates have maintained their hollow-cylindrical shape, and the surface is covered by nanoparticles. This indicates that the temperature reached during reaction was high enough to cause vapor formation, which caused the formation of spherical nanoparticles during cooling. However, this also indicates that the reaction temperature was lower than the melting temperature of Al_2O_3 and Cu_2O (2030 and 1235 °C, respectively), so the structural integrity of the sample was maintained. In contrast, for the reacted 54nm-Cu_2O samples, the hollow-cylinder morphology was not maintained, and the products resemble a melt of cylinders and flakes. This indicates that the reaction temperature was high enough to cause the melting of Al_2O_3 and Cu_2O, and that the thicker Cu_2O layer resulted in a higher bulk temperature during reaction. This visually supports the photodiode data presented in Figure 6-7, where it was shown that increasing the Cu_2O thickness resulted in an increase in energy release.

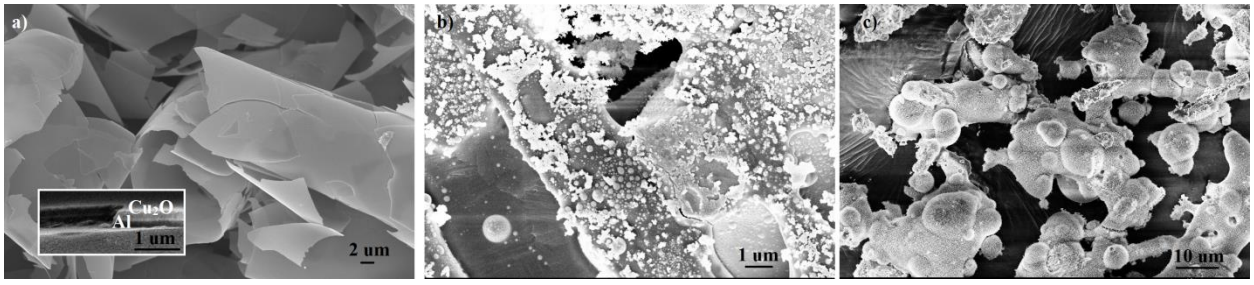

Figure 6-8 SEM images of an a) unreacted sample, b) reacted sample with 45 nm Al and 27 nm Cu_2O, and c) reacted sample with 45 nm Al and 54 nm Cu_2O. From [59]

One further phenomena to discuss is the impact of adding a copper interlayer to the Al/Cu_2O thermite nanolaminates. As discussed in Section 5.3, the copper interlayer imparts improved stability to thin nanolaminate structures, and also lowers the initiation temperature due to the formation of an Al:Cu alloy. For laser ignition, a very thin (~ 10 nm) copper interlayer also yielded a lowering of the ignition delay when added between the Al and Cu_2O layers of the samples. The addition of the copper interlayer was able to bring the minimum ignition delay value from 250 µs to 200 µs for 54nm Cu_2O and 45 nm Al structures. This represents another strategy for tailoring the laser ignition delay of thermite nanolaminates. However, the copper layer thickness should be kept sufficiently small since it can decrease the energy release by reducing the overall content of active material per sample mass.

6.3 Summary

As thermite becomes integrated with MEMs devices, or used for micropropulsion and microwelding, laser will become an ideal source of fast, tunable, wavelength specific, and small-area ignition. Due to this, it is vital to gain an understanding of how thermites can be manipulated to influence factors of laser ignition and reaction. In this case, the influence on ignition delay, initial energy transfer rate (flame spread), and average energy release was explored. Table 2-1 provides a summary of the manipulated properties, and their effect on the ignition and reaction characteristics.

Table 6-1 Summary of the properties, variables affects, and mechanisms by which they are affected during laser ignition

PROPERTY	AFFECTED VARIABLE	MECHANISM
Cu_2O layer thickness	ignition delay	Balance between laser absorption and gaseous oxygen diffusion
	energy release (photodiode signal)	ratio of components
	initial rate of flame area expansion	ratio of components
Al layer thickness	energy release (photodiode signal)	ratio of components
Cu interlayer	ignition delay	alloy formation
	energy release	reduction in active material
substrate	Ignition delay	heat conduction
overall sample thickness	Ignition delay	laser absorption

It was found that varying the thickness of the Al layers had an insignificant effect on the ignition delay. This is due to the fact that the heterogeneous reaction mechanisms of the Al-Cu_2O samples requires the decomposition of the oxide, and diffusion of the gaseous oxygen to the Al-Cu_2O interface, in order to start the exothermic reaction. This makes the movement of oxygen to the Al-Cu_2O interface a rate-limiting step, and is not influenced by the Al thickness.

The Cu_2O thickness showed a u-shaped ignition delay curve with an optimal ignition delay occurring between ~50-70 nm. These experimental results closely follow the theoretical power absorption curve obtained using Lumerical software. This indicates that, at these length scales, the ignition delay is highly dependent on the laser absorption and interaction with the Cu_2O. This differs from macroscale layered materials, where mass diffusion plays a more significant role in determining the ignition delay.

The Cu_2O and Al layer thicknesses play a role on the energy release and rates of flame expansion due to thickness variations resulting in a change in the equivalence ratio. As the ratio of the components approaches the optimal stoichiometry, the energy release is enhanced. Additionally, the flame expansion rate is improved as the ratio of components approaches the optimal equivalence ratio for flame expansion.

The addition of a thin Cu layer at the interface between the Cu_2O and Al layers results in a further reduction of the ignition delay. This can be attributed to the alloying of Al and Cu, and is a strategy that can be used to further manipulate the ignition characteristics of Al-Cu_2O nanolaminates.

7.0 Conclusions, Contributions, and Future Work

7.1 Conclusions

A novel mechanism for determining the reaction mechanism of thermite nanolaminates was developed and presented in Section 4. Utilizing a substrate that becomes sufficiently soft during the heating phase allows for bubbles of generated gas to be captured and stored for analysis. In the case of Al-Cu_2O nanolaminates, bubbles were formed at the thermite-substrate interface, and nanoparticles formed on the surface. The formation of particles was attributed to the vaporization of metals, due to the high heat of reaction, which then nucleate and form particles as they cool. Using EDX analysis, the composition of the bubbles was found to contain no significant metal concentration. This was used as evidence to support that bubble formation was due to oxygen gas being produced, and not due to the vaporization of metals. Since a critical step of the heterogeneous reaction mechanism involves the decomposition of the oxide to produce gaseous oxygen, this support that Al-Cu_2O undergoes a heterogeneous reaction mechanism. Additionally, DSC and TGA data support a heterogeneous reaction mechanism by showing an increase in mass loss occurring before the beginning of the exothermic reaction. This supports that the oxide undergoes a decomposition step (some oxygen is lost to the environment, resulting in the increase in mass loss), and helps to validate that Al-Cu_2O nanolaminates follow a heterogeneous reaction mechanism.

DSC and TGA were used to heat Al-Cu_2O nanolaminates, and record the exothermic/endothermic events and mass loss events. Shrinking the Cu_2O layers resulted in a shift of the reaction peak to lower temperatures. The addition of a Cu interlayer between the Al and Cu_2O layers also resulted in a lower ignition temperature due to alloying between the Al and Cu.

Interestingly, the choice of reaction gas had a large effect on the ignition temperature and energy release of the nanolaminates. The presence of air caused a decrease in the ignition temperature and an increase in the energy release of the samples. This showed that the reaction environment should be a consideration when designing application-specific nanolaminates.

A laser ignition study of Al-Cu_2O thermite nanolaminates was presented in Section 6. The ignition delay, rate of flame expansion, and energy release were evaluated for different thicknesses of Cu_2O. It was found that the energy release and rate of flame expansion increased as the thickness of the Cu_2O increased, which is due to the fact that the Al to Cu_2O ratio is approaching the ideal. It was shown that varying the layer thickness of Al had insignificant effect on the ignition delay, which was related to the fact that this is a heterogeneous reaction mechanism. Due to this, the release and transport of oxygen from the Cu_2O layer is the critical step, and varying the Al layer thickness should have little impact on the release and transport of oxygen. A u-shaped ignition delay curve was found when varying the thickness of the Cu_2O layers, and the minimum ignition delay occurred in the range of ~50-70 nm. A 2D laser absorption model was created with Lumerical software, and utilized to find a relationship between Cu_2O thickness in the nanolaminate and the total power absorption. This model can be compared to the experimental results since the minimum ignition delay should occur at the maximum power absorption. The model showed a similar u-shape trend to the experimental results, but was slightly shifted to lower thickness values (maximum power absorption occurring at ~42nm). This shift could be due to the fact that the properties of sputtered Cu_2O can differ from the Cu_2O in the Lumerical database, the model does not take into account the presence of the Al_2O_3 region and intermixed regions at the interface, and the model does not take into account the thin surface layer of CuO. It should also be noted that incorporating a Cu layer

between the Al and Cu_2O layers lowered the ignition delay, and could be used as a strategy to further manipulate the ignition characteristics.

7.2 Contributions

The contributions of this work can be noticed through addressing the following gaps in literature. Firstly, no in-depth analysis of the reaction mechanism of Al-Cu_2O has been conducted, even though it is a critical step in the popular Al-CuO thermite reaction. Project one not only addresses this gap by determining that Al-Cu_2O nanolaminates undergo a heterogeneous reaction mechanism, but provides a novel method for determining the reaction mechanisms of nanolaminates. This developed method addresses the difficulty of determining the reaction mechanism, as the exothermic reaction can pose risks to equipment, and negates the need for TEM studies. It can also help to further validate DSC results, which can be prone to interpretation error.

Laser ignition continues to gain interest due to its compatibility with MEMs, tunability of power density, tunability of spot size, and range of wavelength to choose from. However, there are few laser ignition studies, and none focus directly on aluminum-copper oxide based nanolaminates. This research gap is addressed in Section 6, where the effect of structural properties on the ignition and reaction characteristics was discussed. For propulsion applications in particular, having a small ignition delay is critical. This work addresses the need for controllable ignition delays by showing that the ignition delay can be tunable through varying the Cu_2O thickness or adding a Cu interlayer.

Finally, Section 4 discusses that ignition and reaction properties of nanolaminates that are heated in DSC. A relationship between Cu_2O thickness and the presence of a Cu interlayer was found, and directly contributed to the gap of understanding Al-Cu_2O nanolaminate reactions. Additionally, it was shown that the gas present in the reaction environment (air of argon) had an

effect on the energy release and ignition temperature. This shows that it is vital to consider the reaction environment when designing thermite nanolaminates. For example, thermite-based propulsion systems may have different properties in space or underwater compared to its use in an environment where it has access to oxygen.

7.3 Future Work

The novel method developed in this work is a promising way of analyzing the reaction mechanisms of thermite nanolaminates. However, the limitations of this method has not been explored. Future work should be carried out to explore compatibility with other thermite types. This method could also be applied to non-thermite materials to collect gas produced during reaction, and this should be validated.

In regards to the copper interlayer, activation energy tests for different copper layer thicknesses should be performed in DSC. The activation energy is a key parameter of the reaction mechanism, and would further quantify the improvements offered by the incorporation of the thin Cu layer. With this, conclusions on optimal Cu layer thickness can be drawn. Additionally, different metal interlayers should be explored.

The laser ignition tests should be repeated for a different thermite formulation (ie: Al-NiO or Al-Fu2O3). It was shown that the ignition delay was greatly affected by the thickness of the Cu_2O layer, creating a u-shaped ignition delay curve. This u-shaped curve was also obtained when using Lumerical software to model the laser power absorption with varying Cu_2O thicknesses. This absorption curve is obtained based on the unique properties of Cu_2O (such as refractive index and permittivity), and would change when switching to another material. Thus, to widen the understanding of nanolaminate ignition, different materials should be characterized.

Copyright Permission

JOHN WILEY AND SONS LICENSE TERMS AND CONDITIONS

Jul 25, 2018

This Agreement between Ms. Lauren LeSergent ("You") and John Wiley and Sons ("John Wiley and Sons") consists of your license details and the terms and conditions provided by John Wiley and Sons and Copyright Clearance Center.

License Number	4395470320985
License date	Jul 24, 2018
Licensed Content Publisher	John Wiley and Sons
Licensed Content Publication	Advanced Functional Materials
Licensed Content Title	High-Energy Al/CuO Nanocomposites Obtained by DNA-Directed Assembly
Licensed Content Author	Fabrice Séverac, Pierre Alphonse, Alain Estève, et al
Licensed Content Date	Oct 18, 2011
Licensed Content Volume	22
Licensed Content Issue	2
Licensed Content Pages	7
Type of use	Dissertation/Thesis
Requestor type	University/Academic
Format	Print and electronic
Portion	Figure/table
Number of figures/tables	1
Original Wiley figure/table number(s)	Figure 1
Will you be translating?	No
Title of your thesis / dissertation	Tailoring the Ignition and Reaction Properties of Cu2O Thermite Nanolaminates
Expected completion date	Jul 2018
Expected size (number of pages)	100
Requestor Location	Ms. Lauren LeSergent 155 Park St Waterloo, ON N2L1Y5

	Canada Attn: Ms. Lauren LeSergent
Publisher Tax ID	EU826007151
Total	0.00 CAD
Terms and Conditions	

TERMS AND CONDITIONS

This copyrighted material is owned by or exclusively licensed to John Wiley & Sons, Inc. or one of its group companies (each a"Wiley Company") or handled on behalf of a society with which a Wiley Company has exclusive publishing rights in relation to a particular work (collectively "WILEY"). By clicking "accept" in connection with completing this licensing transaction, you agree that the following terms and conditions apply to this transaction (along with the billing and payment terms and conditions established by the Copyright Clearance Center Inc., ("CCC's Billing and Payment terms and conditions"), at the time that you opened your RightsLink account (these are available at any time at http://myaccount.copyright.com).

Terms and Conditions

- The materials you have requested permission to reproduce or reuse (the "Wiley Materials") are protected by copyright.

- You are hereby granted a personal, non-exclusive, non-sub licensable (on a stand-alone basis), non-transferable, worldwide, limited license to reproduce the Wiley Materials for the purpose specified in the licensing process. This license, **and any CONTENT (PDF or image file) purchased as part of your order,** is for a one-time use only and limited to any maximum distribution number specified in the license. The first instance of republication or reuse granted by this license must be completed within two years of the date of the grant of this license (although copies prepared before the end date may be distributed thereafter). The Wiley Materials shall not be used in any other manner or for any other purpose, beyond what is granted in the license. Permission is granted subject to an appropriate acknowledgement given to the author, title of the material/book/journal and the publisher. You shall also duplicate the copyright notice that appears in the Wiley publication in your use of the Wiley Material. Permission is also granted on the understanding that nowhere in the text is a previously published source acknowledged for all or part of this Wiley Material. Any third party content is expressly excluded from this permission.

- With respect to the Wiley Materials, all rights are reserved. Except as expressly granted by the terms of the license, no part of the Wiley Materials may be copied, modified, adapted (except for minor reformatting required by the new Publication), translated, reproduced, transferred or distributed, in any form or by any means, and no derivative works may be made based on the Wiley Materials without the prior permission of the respective copyright owner.**For STM Signatory Publishers clearing permission under the terms of the STM Permissions Guidelines only, the terms of the license are extended to include subsequent editions and for editions in other languages, provided such editions are for the work as a whole in situ and does not involve the separate exploitation of the**

permitted figures or extracts,You may not alter, remove or suppress in any manner any copyright, trademark or other notices displayed by the Wiley Materials. You may not license, rent, sell, loan, lease, pledge, offer as security, transfer or assign the Wiley Materials on a stand-alone basis, or any of the rights granted to you hereunder to any other person.

- The Wiley Materials and all of the intellectual property rights therein shall at all times remain the exclusive property of John Wiley & Sons Inc, the Wiley Companies, or their respective licensors, and your interest therein is only that of having possession of and the right to reproduce the Wiley Materials pursuant to Section 2 herein during the continuance of this Agreement. You agree that you own no right, title or interest in or to the Wiley Materials or any of the intellectual property rights therein. You shall have no rights hereunder other than the license as provided for above in Section 2. No right, license or interest to any trademark, trade name, service mark or other branding ("Marks") of WILEY or its licensors is granted hereunder, and you agree that you shall not assert any such right, license or interest with respect thereto

- NEITHER WILEY NOR ITS LICENSORS MAKES ANY WARRANTY OR REPRESENTATION OF ANY KIND TO YOU OR ANY THIRD PARTY, EXPRESS, IMPLIED OR STATUTORY, WITH RESPECT TO THE MATERIALS OR THE ACCURACY OF ANY INFORMATION CONTAINED IN THE MATERIALS, INCLUDING, WITHOUT LIMITATION, ANY IMPLIED WARRANTY OF MERCHANTABILITY, ACCURACY, SATISFACTORY QUALITY, FITNESS FOR A PARTICULAR PURPOSE, USABILITY, INTEGRATION OR NON-INFRINGEMENT AND ALL SUCH WARRANTIES ARE HEREBY EXCLUDED BY WILEY AND ITS LICENSORS AND WAIVED BY YOU.

- WILEY shall have the right to terminate this Agreement immediately upon breach of this Agreement by you.

- You shall indemnify, defend and hold harmless WILEY, its Licensors and their respective directors, officers, agents and employees, from and against any actual or threatened claims, demands, causes of action or proceedings arising from any breach of this Agreement by you.

- IN NO EVENT SHALL WILEY OR ITS LICENSORS BE LIABLE TO YOU OR ANY OTHER PARTY OR ANY OTHER PERSON OR ENTITY FOR ANY SPECIAL, CONSEQUENTIAL, INCIDENTAL, INDIRECT, EXEMPLARY OR PUNITIVE DAMAGES, HOWEVER CAUSED, ARISING OUT OF OR IN CONNECTION WITH THE DOWNLOADING, PROVISIONING, VIEWING OR USE OF THE MATERIALS REGARDLESS OF THE FORM OF ACTION, WHETHER FOR BREACH OF CONTRACT, BREACH OF WARRANTY, TORT, NEGLIGENCE, INFRINGEMENT OR OTHERWISE (INCLUDING, WITHOUT LIMITATION, DAMAGES BASED ON LOSS OF PROFITS, DATA, FILES, USE, BUSINESS OPPORTUNITY OR CLAIMS OF THIRD PARTIES), AND WHETHER OR NOT THE PARTY HAS BEEN ADVISED OF THE POSSIBILITY OF SUCH DAMAGES. THIS LIMITATION SHALL APPLY NOTWITHSTANDING ANY FAILURE OF ESSENTIAL PURPOSE OF ANY LIMITED REMEDY PROVIDED HEREIN.

- Should any provision of this Agreement be held by a court of competent jurisdiction to be illegal, invalid, or unenforceable, that provision shall be deemed amended to achieve as

nearly as possible the same economic effect as the original provision, and the legality, validity and enforceability of the remaining provisions of this Agreement shall not be affected or impaired thereby.

- The failure of either party to enforce any term or condition of this Agreement shall not constitute a waiver of either party's right to enforce each and every term and condition of this Agreement. No breach under this agreement shall be deemed waived or excused by either party unless such waiver or consent is in writing signed by the party granting such waiver or consent. The waiver by or consent of a party to a breach of any provision of this Agreement shall not operate or be construed as a waiver of or consent to any other or subsequent breach by such other party.

- This Agreement may not be assigned (including by operation of law or otherwise) by you without WILEY's prior written consent.

- Any fee required for this permission shall be non-refundable after thirty (30) days from receipt by the CCC.

- These terms and conditions together with CCC's Billing and Payment terms and conditions (which are incorporated herein) form the entire agreement between you and WILEY concerning this licensing transaction and (in the absence of fraud) supersedes all prior agreements and representations of the parties, oral or written. This Agreement may not be amended except in writing signed by both parties. This Agreement shall be binding upon and inure to the benefit of the parties' successors, legal representatives, and authorized assigns.

- In the event of any conflict between your obligations established by these terms and conditions and those established by CCC's Billing and Payment terms and conditions, these terms and conditions shall prevail.

- WILEY expressly reserves all rights not specifically granted in the combination of (i) the license details provided by you and accepted in the course of this licensing transaction, (ii) these terms and conditions and (iii) CCC's Billing and Payment terms and conditions.

- This Agreement will be void if the Type of Use, Format, Circulation, or Requestor Type was misrepresented during the licensing process.

- This Agreement shall be governed by and construed in accordance with the laws of the State of New York, USA, without regards to such state's conflict of law rules. Any legal action, suit or proceeding arising out of or relating to these Terms and Conditions or the breach thereof shall be instituted in a court of competent jurisdiction in New York County in the State of New York in the United States of America and each party hereby consents and submits to the personal jurisdiction of such court, waives any objection to venue in such court and consents to service of process by registered or certified mail, return receipt requested, at the last known address of such party.

WILEY OPEN ACCESS TERMS AND CONDITIONS

Wiley Publishes Open Access Articles in fully Open Access Journals and in Subscription journals offering Online Open. Although most of the fully Open Access journals publish open access articles under the terms of the Creative Commons Attribution (CC BY) License only, the subscription journals and a few of the Open Access Journals offer a choice of Creative Commons Licenses. The license type is clearly identified on the article.

The Creative Commons Attribution License

The Creative Commons Attribution License (CC-BY) allows users to copy, distribute and transmit an article, adapt the article and make commercial use of the article. The CC-BY license permits commercial and non-

Creative Commons Attribution Non-Commercial License

The Creative Commons Attribution Non-Commercial (CC-BY-NC)License permits use, distribution and reproduction in any medium, provided the original work is properly cited and is not used for commercial purposes.(see below)

Creative Commons Attribution-Non-Commercial-NoDerivs License

The Creative Commons Attribution Non-Commercial-NoDerivs License (CC-BY-NC-ND) permits use, distribution and reproduction in any medium, provided the original work is properly cited, is not used for commercial purposes and no modifications or adaptations are made. (see below)

Use by commercial "for-profit" organizations

Use of Wiley Open Access articles for commercial, promotional, or marketing purposes requires further explicit permission from Wiley and will be subject to a fee.

Further details can be found on Wiley Online Library http://olabout.wiley.com/WileyCDA/Section/id-410895.html

Other Terms and Conditions:

v1.10 Last updated September 2015

Questions? customercare@copyright.com or +1-855-239-3415 (toll free in the US) or +1-978-646-2777.

JOHN WILEY AND SONS LICENSE TERMS AND CONDITIONS

Jul 25, 2018

This Agreement between Ms. Lauren LeSergent ("You") and John Wiley and Sons ("John Wiley and Sons") consists of your license details and the terms and conditions provided by John Wiley and Sons and Copyright Clearance Center.

License Number	4395561059323
License date	Jul 24, 2018
Licensed Content Publisher	John Wiley and Sons
Licensed Content Publication	Advanced Engineering Materials
Licensed Content Title	Diversity in Addressing Reaction Mechanisms of Nano-Thermite Composites with a Layer by Layer Structure
Licensed Content Author	Hongtao Sui, Lauren LeSergent, John Z. Wen
Licensed Content Date	Nov 15, 2017
Licensed Content Volume	20
Licensed Content Issue	3
Licensed Content Pages	11
Type of use	Dissertation/Thesis
Requestor type	Author of this Wiley article
Format	Print and electronic
Portion	Figure/table
Number of figures/tables	1
Original Wiley figure/table number(s)	Figure 4
Will you be translating?	No
Title of your thesis / dissertation	Tailoring the Ignition and Reaction Properties of Cu2O Thermite Nanolaminates
Expected completion date	Jul 2018
Expected size (number of pages)	100
Requestor Location	Ms. Lauren LeSergent 155 Park St Waterloo, ON N2L1Y5 Canada Attn: Ms. Lauren LeSergent
Publisher Tax ID	EU826007151

Total 0.00 CAD

Terms and Conditions

TERMS AND CONDITIONS

This copyrighted material is owned by or exclusively licensed to John Wiley & Sons, Inc. or one of its group companies (each a"Wiley Company") or handled on behalf of a society with which a Wiley Company has exclusive publishing rights in relation to a particular work (collectively "WILEY"). By clicking "accept" in connection with completing this licensing transaction, you agree that the following terms and conditions apply to this transaction (along with the billing and payment terms and conditions established by the Copyright Clearance Center Inc., ("CCC's Billing and Payment terms and conditions"), at the time that you opened your RightsLink account (these are available at any time at http://myaccount.copyright.com).

Terms and Conditions

- The materials you have requested permission to reproduce or reuse (the "Wiley Materials") are protected by copyright.

- You are hereby granted a personal, non-exclusive, non-sub licensable (on a stand-alone basis), non-transferable, worldwide, limited license to reproduce the Wiley Materials for the purpose specified in the licensing process. This license, **and any CONTENT (PDF or image file) purchased as part of your order,** is for a one-time use only and limited to any maximum distribution number specified in the license. The first instance of republication or reuse granted by this license must be completed within two years of the date of the grant of this license (although copies prepared before the end date may be distributed thereafter). The Wiley Materials shall not be used in any other manner or for any other purpose, beyond what is granted in the license. Permission is granted subject to an appropriate acknowledgement given to the author, title of the material/book/journal and the publisher. You shall also duplicate the copyright notice that appears in the Wiley publication in your use of the Wiley Material. Permission is also granted on the understanding that nowhere in the text is a previously published source acknowledged for all or part of this Wiley Material. Any third party content is expressly excluded from this permission.

- With respect to the Wiley Materials, all rights are reserved. Except as expressly granted by the terms of the license, no part of the Wiley Materials may be copied, modified, adapted (except for minor reformatting required by the new Publication), translated, reproduced, transferred or distributed, in any form or by any means, and no derivative works may be made based on the Wiley Materials without the prior permission of the respective copyright owner.**For STM Signatory Publishers clearing permission under the terms of the STM Permissions Guidelines only, the terms of the license are extended to include subsequent editions and for editions in other languages, provided such editions are for the work as a whole in situ and does not involve the separate exploitation of the permitted figures or extracts,**You may not alter, remove or suppress in any manner any copyright, trademark or other notices displayed by the Wiley Materials. You may not license, rent, sell, loan, lease, pledge, offer as security, transfer or assign the Wiley

Materials on a stand-alone basis, or any of the rights granted to you hereunder to any other person.

- The Wiley Materials and all of the intellectual property rights therein shall at all times remain the exclusive property of John Wiley & Sons Inc, the Wiley Companies, or their respective licensors, and your interest therein is only that of having possession of and the right to reproduce the Wiley Materials pursuant to Section 2 herein during the continuance of this Agreement. You agree that you own no right, title or interest in or to the Wiley Materials or any of the intellectual property rights therein. You shall have no rights hereunder other than the license as provided for above in Section 2. No right, license or interest to any trademark, trade name, service mark or other branding ("Marks") of WILEY or its licensors is granted hereunder, and you agree that you shall not assert any such right, license or interest with respect thereto

- NEITHER WILEY NOR ITS LICENSORS MAKES ANY WARRANTY OR REPRESENTATION OF ANY KIND TO YOU OR ANY THIRD PARTY, EXPRESS, IMPLIED OR STATUTORY, WITH RESPECT TO THE MATERIALS OR THE ACCURACY OF ANY INFORMATION CONTAINED IN THE MATERIALS, INCLUDING, WITHOUT LIMITATION, ANY IMPLIED WARRANTY OF MERCHANTABILITY, ACCURACY, SATISFACTORY QUALITY, FITNESS FOR A PARTICULAR PURPOSE, USABILITY, INTEGRATION OR NON-INFRINGEMENT AND ALL SUCH WARRANTIES ARE HEREBY EXCLUDED BY WILEY AND ITS LICENSORS AND WAIVED BY YOU.

- WILEY shall have the right to terminate this Agreement immediately upon breach of this Agreement by you.

- You shall indemnify, defend and hold harmless WILEY, its Licensors and their respective directors, officers, agents and employees, from and against any actual or threatened claims, demands, causes of action or proceedings arising from any breach of this Agreement by you.

- IN NO EVENT SHALL WILEY OR ITS LICENSORS BE LIABLE TO YOU OR ANY OTHER PARTY OR ANY OTHER PERSON OR ENTITY FOR ANY SPECIAL, CONSEQUENTIAL, INCIDENTAL, INDIRECT, EXEMPLARY OR PUNITIVE DAMAGES, HOWEVER CAUSED, ARISING OUT OF OR IN CONNECTION WITH THE DOWNLOADING, PROVISIONING, VIEWING OR USE OF THE MATERIALS REGARDLESS OF THE FORM OF ACTION, WHETHER FOR BREACH OF CONTRACT, BREACH OF WARRANTY, TORT, NEGLIGENCE, INFRINGEMENT OR OTHERWISE (INCLUDING, WITHOUT LIMITATION, DAMAGES BASED ON LOSS OF PROFITS, DATA, FILES, USE, BUSINESS OPPORTUNITY OR CLAIMS OF THIRD PARTIES), AND WHETHER OR NOT THE PARTY HAS BEEN ADVISED OF THE POSSIBILITY OF SUCH DAMAGES. THIS LIMITATION SHALL APPLY NOTWITHSTANDING ANY FAILURE OF ESSENTIAL PURPOSE OF ANY LIMITED REMEDY PROVIDED HEREIN.

- Should any provision of this Agreement be held by a court of competent jurisdiction to be illegal, invalid, or unenforceable, that provision shall be deemed amended to achieve as nearly as possible the same economic effect as the original provision, and the legality,

validity and enforceability of the remaining provisions of this Agreement shall not be affected or impaired thereby.

- The failure of either party to enforce any term or condition of this Agreement shall not constitute a waiver of either party's right to enforce each and every term and condition of this Agreement. No breach under this agreement shall be deemed waived or excused by either party unless such waiver or consent is in writing signed by the party granting such waiver or consent. The waiver by or consent of a party to a breach of any provision of this Agreement shall not operate or be construed as a waiver of or consent to any other or subsequent breach by such other party.

- This Agreement may not be assigned (including by operation of law or otherwise) by you without WILEY's prior written consent.

- Any fee required for this permission shall be non-refundable after thirty (30) days from receipt by the CCC.

- These terms and conditions together with CCC's Billing and Payment terms and conditions (which are incorporated herein) form the entire agreement between you and WILEY concerning this licensing transaction and (in the absence of fraud) supersedes all prior agreements and representations of the parties, oral or written. This Agreement may not be amended except in writing signed by both parties. This Agreement shall be binding upon and inure to the benefit of the parties' successors, legal representatives, and authorized assigns.

- In the event of any conflict between your obligations established by these terms and conditions and those established by CCC's Billing and Payment terms and conditions, these terms and conditions shall prevail.

- WILEY expressly reserves all rights not specifically granted in the combination of (i) the license details provided by you and accepted in the course of this licensing transaction, (ii) these terms and conditions and (iii) CCC's Billing and Payment terms and conditions.

- This Agreement will be void if the Type of Use, Format, Circulation, or Requestor Type was misrepresented during the licensing process.

- This Agreement shall be governed by and construed in accordance with the laws of the State of New York, USA, without regards to such state's conflict of law rules. Any legal action, suit or proceeding arising out of or relating to these Terms and Conditions or the breach thereof shall be instituted in a court of competent jurisdiction in New York County in the State of New York in the United States of America and each party hereby consents and submits to the personal jurisdiction of such court, waives any objection to venue in such court and consents to service of process by registered or certified mail, return receipt requested, at the last known address of such party.

WILEY OPEN ACCESS TERMS AND CONDITIONS

Wiley Publishes Open Access Articles in fully Open Access Journals and in Subscription journals offering Online Open. Although most of the fully Open Access journals publish

open access articles under the terms of the Creative Commons Attribution (CC BY) License only, the subscription journals and a few of the Open Access Journals offer a choice of Creative Commons Licenses. The license type is clearly identified on the article.

The Creative Commons Attribution License

The Creative Commons Attribution License (CC-BY) allows users to copy, distribute and transmit an article, adapt the article and make commercial use of the article. The CC-BY license permits commercial and non-

Creative Commons Attribution Non-Commercial License

The Creative Commons Attribution Non-Commercial (CC-BY-NC)License permits use, distribution and reproduction in any medium, provided the original work is properly cited and is not used for commercial purposes.(see below)

Creative Commons Attribution-Non-Commercial-NoDerivs License

The Creative Commons Attribution Non-Commercial-NoDerivs License (CC-BY-NC-ND) permits use, distribution and reproduction in any medium, provided the original work is properly cited, is not used for commercial purposes and no modifications or adaptations are made. (see below)

Use by commercial "for-profit" organizations

Use of Wiley Open Access articles for commercial, promotional, or marketing purposes requires further explicit permission from Wiley and will be subject to a fee.

Further details can be found on Wiley Online Library http://olabout.wiley.com/WileyCDA/Section/id-410895.html

Other Terms and Conditions:

v1.10 Last updated September 2015

Questions? customercare@copyright.com or +1-855-239-3415 (toll free in the US) or +1-978-646-2777.

Title: Electrospun Nanofiber-Based Thermite Textiles and their Reactive Properties

Author: Shi Yan, Guoqiang Jian, Michael R. Zachariah

Publication: Applied Materials

Publisher: American Chemical Society

Date: Dec 1, 2012

PERMISSION/LICENSE IS GRANTED FOR YOUR ORDER AT NO CHARGE

This type of permission/license, instead of the standard Terms & Conditions, is sent to you because no fee is being charged for your order. Please note the following:

- Permission is granted for your request in both print and electronic formats, and translations.
- If figures and/or tables were requested, they may be adapted or used in part.
- Please print this page for your records and send a copy of it to your publisher/graduate school.
- Appropriate credit for the requested material should be given as follows: "Reprinted (adapted) with permission from (COMPLETE REFERENCE CITATION). Copyright (YEAR) American Chemical Society." Insert appropriate information in place of the capitalized words.
- One-time permission is granted only for the use specified in your request. No additional uses are granted (such as derivative works or other editions). For any other uses, please submit a new request.

If credit is given to another source for the material you requested, permission must be obtained from that source.

References

[1] S. J. Apperson, A. V. Bezmelnitsyn, R. Thiruvengadathan, K. Gangopadhyay, S. Gangopadhyay, W. A. Balas, P. E. Anderson and S. M. Nicolich, "Characterization of nanothermite materials for solid-fuel microthruster applications," *J. Propul. Power,* vol. 25, no. 5, pp. 1086-1091, 2009.

[2] C. Rossi, K. Zhang, D. Estève, A. P., P. Tailhades and C. Vahlas, "Nanoenergetic materials for MEMS: a review," *J. Microelectromech. Syst.,* vol. 16, no. 4, pp. 919-931, 2007.

[3] M. Petrantoni, C. Rossi, L. Salvagnac, C. V., A. Estève, C. Tenailleau, P. Alphonse and Y. J. Chabal, "Multilayered Al/CuO thermite formation by reactive magnetron sputtering: Nano versus micro," *J. Appl. Phys.,* vol. 108, 2010.

[4] E. L. Routh, Engineering reactivity in thermite reactive nano-laminates, Raleigh, NC: North Carolina State University, 2018.

[5] E. Lafontaine and M. Comet, Nanothermites, London: ISTE Ltd, 2016.

[6] M. L. Pantoya and J. J. Granier, "Combustion behaviour of highly energetic thermites: nano versus micron composites," *Propellants, Explos., Pyrotech.,* vol. 30, pp. 53-62, 2005.

[7] C. E. Aumann, G. L. Skofronick and J. A. Martin, "Oxidation behaviour of aluminum nanopowders," *J. Vac. Sci. Technol. B,* vol. 13, p. 1178, 1995.

[8] E. J. Mily, A. Oni, J. M. LeBeau, Y. Liu, H. J. Brown-Shaklee, J. F. Ihlefeld and J. -P. Maria, "The role of terminal oxide structure and properties in nanothermite reactions," *Thin Solid Films,* vol. 562, pp. 405-410, 2014.

[9] G. Bohlouli Zanjani, Synthesis, characterization, and application of nanothermites for joining, University of Waterloo, 2013.

[10] S. H. Fischer and M. C. Grubelich, "Theoretical energy release of thermites, intermetallics, and combustible metals," *The 24th International Pyrotechnics Seminar,* 1998.

[11] K. Zhang, C. Rossi, P. Alphonse, C. Tenailleau, S. Cayez and J. -Y. Chane-Ching, "Integrating Al with NiO nano honeycomb to realize an energetic material on silicon substrate," *Appl. Phys. A,* vol. 94, no. 4, pp. 957-962, 2009.

[12] O. B. Kubaschewski, C. B. Alcock and P. J. Spencer, Materials Thermochemistry, 6th ed., Oxford, New York: Pergamon Press, 1993.

[13] V. Baijot, L. Glavier, J. -M. Ducéré, M. Djafari-Rouhani, C. Rossi and A. Estève, "Modeling the pressure generation in aluminum based thermites," *Propellants Explos. Pyrotech,* vol. 40, no. 3, pp. 402-412, 2015.

[14] I. Abdallah, J. Zapata, G. Lahiner, B. Warot-Fonrose, J. Cure, Y. Chabal, A. Estève and C. Rossi, "Structure and chemical characterization at the atomic level of reactions in Al/CuO multilayers," *ACS Appl. Energy Mater.,* vol. 1, no. 4, pp. 1762-1770, 2018.

[15] G. Lahiner, A. Nicollet, J. Zapata, L. Marin, N. Richard, M. Djafari-Rouhani, C. Rossi and A. Estève, "A diffusion-reaction scheme for modeling ignition and self-propagating reactions in Al/CuO multilayered thin-films," *J. Appl. Phys.,* vol. 122, 2017.

[16] A. H. Kinsey, K. Slusarski, S. Sosa and T. P. Weihs, "Gas suppression via copper interlayers in magnetron sputtered Al-Cu2O multilayers," *ACS Appl. Mater. Interfaces,* vol. 9, no. 26, pp. 22026-22036, 2017.

[17] A. Nicollet, G. Lahiner, A. Belisario, S. S., M. Djafari-Rouhani, A. Estève and C. Rossi, "Investigation of Al/CuO multilayered thermite ignition," *J. Appl. Phys.,* vol. 121, 2017.

[18] L. Marín, Y. Gao, M. Vallet, I. Abdallah, B. Warot-Fonrose, C. Tenailleau, T. Lucero, J. Kim, A. Esteve, Y. J. Chabal and C. Rossi, "Performance enhancement via incorporation of ZnO nanolayers in energetic Al/CuO multilayers," *Langmuir,* vol. 33, pp. 11086-11093, 2017.

[19] J. B. DeLisio, F. Yi, D. LaVan and M. R. Zachariah, "High heating rate reaction dynamics of Al/CuO nanolaminates by nanocalorimetry-coupled time-of-flight mass spectroscopy," *J. Phys. Chem.,* vol. 121, pp. 2771-2777, 2017.

[20] L. Marín, B. Warot-Fonrose, A. Estève, Y. J. Chabal, L. A. Rodriguez and C. Rossi, "Self-organized Al2Cu nanocrystals at the interface of aluminum-based reactive nanolaminates to lower reaction onset temperature," *ACS Appl. Mater. Interfaces,* vol. 8, pp. 13104-13113, 2016.

[21] L. Marín, N. C. E., J. -F. Veyan, B. Warot-Fonrose, S. Joulie, A. Estève, C. Tenailleau, C. Y. J. and C. Rossi, "Enhancing the reactivity of Al/CuO nanolaminates by Cu incorporation at the interfaces," *ACS Appl. Mater. Interfaces,* vol. 7, pp. 11713-11718, 2015.

[22] Y. Li, Y. Gao, X. Jia, B. Zhou and R. -Q. Shen, "Fabrication and performances of Al/CuO nano composite films for ignition application," *Mater. Sci. Eng.,* vol. 87, p. 012102, 2015.

[23] G. C. Egan, E. J. Mily, J. -P. Maria and M. R. Zachariah, "Probing the reaction dynamics of thermite nanolaminates," *J. Phys. Chem. C. ,* vol. 119, pp. 20401-20408, 2015.

[24] M. Bahrami, G. Taton, V. Conédéra, L. Salvagnac, C. Tenailleau, P. Alphonse and C. Rossi, "Magnetron sputtered Al-CuO nanolaminates: effect of stoichiometry and layers thickness on energy release and burning rate," *Propellants Explos. Pyrotech. ,* vol. 39, pp. 365-373, 2014.

[25] J. Kwon, J. M. Ducéré, P. Alphonse, M. Bahrami, M. Petrantoni, J. -F. Veyan, C. Tenailleau, A. Estève, C. Rossi and Y. J. Chabal, "Interfacial chemistry in Al/CuO reactive nanomaterials and its role in exothermic reaction," *ACS Appl. Mater. Interfaces,* vol. 5, pp. 605-613, 2013.

[26] P. Zhu, R. Shen, Y. Ye, X. Zhou and Y. Hu, "Energetic igniters realized by integrating Al/CuO reactive multilayer films with Cr films," *J. Appl. Phys.,* vol. 110, p. 074513, 2011.

[27] N. A. Manesh, S. Basu and R. Kumar, "Experimental flame speed in multi-layered nano-energetic materials," *Combust. Flame,* vol. 157, pp. 476-480, 2010.

[28] K. J. Blobaum, M. E. Reiss, J. M. Plitzko and T. P. Weihs, "Deposition and characterisation of a self-propagating CuOx/Al thermite reaction in a multilayer foil geometry," *J. Appl. Phys.,* vol. 94, no. 5, pp. 2915-2922, 2003.

[29] K. J. Blobaum, A. J. Wagner, J. M. Plitzko, D. Van Heerden, D. H. Fairbrother and T. P. Weihs, "Investigating the reaction path and growth kinetics in CuOx/Al multilayer foils," *J. Appl. Phys.,* vol. 94, no. 5, pp. 2923-2929, 2003.

[30] T. N. Taylor and J. A. Martin, "Reaction of vapor-deposited aluminum with copper oxides," *J. Vac. Sci. Technol. A,* vol. 9, no. 3, pp. 1840-1846, 1991.

[31] Y. Meir and E. Jerby, "Underwater microwave ignition of hydrophobic thermite powder enabled by the bubble-marble effect," *Appl. Phys. Lett.,* vol. 107, no. 5, p. 054101, 2015.

[32] C. Bodsworth, The extraction and refining of metals, New York: Boca Raton, FL, 1994.

[33] D. S. Hacker and P. Lieberman, "Thermodynamic performance evaluation of a hydroduct using a thermite fuel," *J. Hydronautics,* vol. 3, no. 3, pp. 139-144, 1969.

[34] A. Gash, T. Barbee and O. Cervantes, "Stab sensitivity of energetic nanolaminates," in *33rd International Pyrotechnic Seminar*, Fort Collins, CO, 2006.

[35] S. J. Apperson, A. V. Bezmelnitsyn, R. Thiruvengadathan, K. Gangopadhyay, S. Gangopadhyay, W. A. Balas, P. E. Anderson and S. M. Nicolich, "Characterization of nanothermite materials for solid-fuel microthruster applications," *J. Propul. Power,* vol. 25, no. 5, pp. 1086-1091, 2009.

[36] S. Apperson, R. Thiruvengadathan, K. Bezmelnitsyn, K. Gangopadhyay, S. Gangopadhyay and L. Polo-Parada, "Nanothermite-based microsystem for drug delivery and cell transfection," 2008.

[37] A. Lopez, A. Drukier, K. Freese, C. Murdak and G. Tarle, "New dark matter detectors using nanoscale explosives," University of Michigan, Ann Arbor, MI, 2014.

[38] L. Qin, T. Gong, H. Hao, K. Wang and H. Feng, "Core-shell-structured nanothermites synthesized by atomic layer deposition," *J. Nanopart. Res.,* vol. 15, p. 2150, 2013.

[39] H. Wang, G. Jian, G. C. Egan and R. Zachariah, "Assembly and reactive properties of Al/CuO based nanothermite microparticles," *Combust. Flame,* vol. 161, pp. 2203-2208, 2014.

[40] S. Yan, G. Jian and M. R. Zachariah, "Electrospun nanofiber-based thermite textiles and their reactive properties," *Appl. Mater. Interfaces,* vol. 4, pp. 6432-6435, 2012.

[41] T. M. Tillotson, A. E. Gash, R. L. Simpson, L. W. Hrubesh, J. H. Satcher Jr and J. F. Poco, "Nanostructured energetic materials using sol-gel methodologies," *J. Non-Cryst. Solids,* vol. 285, no. 1-3, pp. 338-345, 2001.

[42] H. Sui, L. LeSergent and J. Z. Wen, "Diversity in addressing reaction mechanisms of nano-thermite composites with a layer by layer structure," *Adv. Eng. Mater.,* vol. 20, no. 3, 2017.

[43] K. T. Sullivan, M. A. Worsley, J. D. Kuntz and A. E. Gash, "Electrophoretic deposition of binary energetic composites," *Combust. Flame,* vol. 159, pp. 2210-2218, 2012.

[44] K. T. Sillivan, J. D. Kuntz and A. E. Gash, "Electrophoretic deposition and mechanistic studies of nano-Al/CuO thermites," *J. Appl. Phys.,* vol. 112, 2012.

[45] R. Shende, S. Subramanian, S. Hasan, S. Apperson, R. Thiruvengadathan, K. Gangopadhyay and G. S., "Nanoenergetic composites of CuO nanorods, nanowires, and Al-nanoparticles," *Propellants Explos. Pyrotech.,* vol. 33, no. 2, pp. 122-130, 2008.

[46] F. Séverac, P. Alphonse, A. Estève, A. Bancaud and C. Rossi, "High-energy Al/CuO nanocomposites obtained by DNA-directed assembly," *Adv. Funct. Mater.,* vol. 22, pp. 323-329, 2012.

[47] X. Zhou, M. Torabi, J. Lu, R. Shen and K. Zhang, "Nanostructured energetic composites: synthesis, ignition/combustion modeling, and applications," *ACS Appl. Mater. Interfaces,* vol. 6, pp. 3058-3074, 2014.

[48] A. S. Rogachev and A. S. Mukasyan, "Combustion of heterogeneous nanostructural systems (Review)," *Combust. Explos. Shock Waves,* vol. 46, no. 3, 2010.

[49] S. K. Chou, W. M. Yang, K. J. Chua, J. Li and K. L. Zhang, "Development of micro power generators - a review," *Appl. Energy,* vol. 88, pp. 1-16, 2011.

[50] F. Bensebaa, "Nanoparticle technologies from lab to market," *Interface Sci. and Tech.,* vol. 19, pp. 279-383, 2013.

[51] R. J. Jacob, D. L. Oritz-Montalvo, K. R. Overdeep, T. P. Weihs and M. R. Zachariah, "Incomplete reactions in nanothermite composites," *J. Appl. Phys.,* vol. 121, p. 054307, 2017.

[52] K. T. Sullivan, W.-A. Chiou, R. Fiore and M. R. Zachariah, "In situ microscopy of rapidly heated nano-Al and nano-Al/WO3 thermites," *Appl. Phys. Lett.,* vol. 97, p. 133104, 2012.

[53] G. C. Egan, T. LaGrange and M. R. Zachariah, "Time-resolved nanosecond imaging of nanoscale condensed phase reaction," *J. Phys. Chem.,* vol. 119, pp. 2792-2797, 2015.

[54] N. W. Piekiel, L. Zhou, K. T. Sullivan, S. Chowdhury, G. C. Egan and M. R. Zachariah, "Initiation and reaction in Al/Bi2O3 nanothermites: evidence for the predominance of condensed phase chemistry," *Combust. Sci. Technol.,* vol. 186, pp. 1209-1224, 2014.

[55] R. J. Jacob, G. Jian, P. M. Guerieri and M. R. Zachariah, "Energy release pathways in nanothermites follow through the condensed state," *Combust. Flame,* vol. 162, pp. 258-264, 2015.

[56] M. J. O'Neil and e. al., The merck index-an encyclopedia of chemicals, drugs, and biologicals, 13th edition, Whitehouse Station, NJ: Merch and Co., 2001.

[57] S. Budavari and e. al., The merck index-an encyclopedia of chemicals, drugs, and biologicals, Whitehouse Station, NJ: Merck and Co., Inc., 1996.

[58] K. Zhang, C. Rossi, G. A. Ardilla Rodriguez, C. Tenailleau and P. Alphonse, "Development of nano-Al/CuO based energetic material on silicon substrate," *Appl. Phys. Letters,* vol. 91, no. 11, p. 3117, 2007.

[59] F. Saceleanu, L. LeSergent, H. Sui and J. Z. Wen, "Low-power laser ignition of aluminum/copper oxide nanothermite structures," in *CICS Spring Technical Meeting 2018*, Toronto, ON, 2018.

[60] Lumerical Inc., "Simple Method," 2003-2018. [Online]. Available: https://kb.lumerical.com/en/index.html?layout_analysis_pabs_simple.html.

[61] J. B. Schneider, "Understanding the finite-difference time-domain method," 2010. [Online]. Available: www.eecs.wsu.edu/~schneidj/ufdtd.

[62] Thermo Fisher Scientific Inc., "Copper," Thermo Scientific , 2018. [Online]. Available: https://xpssimplified.com/elements/copper.php. [Accessed 25 July 2018].

[63] W. He, P. -J. Liu, G.-Q. He, M. Gozin and Q. -L. Yan, "Highly reactive metastable intermixed composites (MICs): preparation and characterization," *Adv. Mater,* p. 1706293, 2018.

[64] N. Ramadan, K. Tur and E. Konca, "Process design optimization for welding of the head hardened R350 Ht rails and their fatigue: a literature review," *IJERD,* vol. 13, no. 1, pp. 49-55, 2017.

[65] D. R. Lide and e. al., CRC Handbook of Chemistry and Physics. 79th ed., Boca Raton, FL: CRC Press Inc, 1998.

[66] R. C. Weast and e. al., Handbook of chemistry and physics, 68th ed., Boca Raton, FL: CRC Press Inc., 1987.

[67] R. J. Lewis, Hawley's condensed chemical dictionary 15th edition, New York, NY: John Wiley & Sonc, Inc, 2007.

[68] R. J. Lewis, Sax's dangerous properties of industrial materials, 11th edition, Hoboken, NJ: Wiley-Interscience, Wiley & Sons, Inc, 2004.

Appendix A

Detailed Procedures

Cleaning substrates

1) Place substrate in beaker
2) Pour isopropyl alcohol and acetone on top of the substrate, until covered, and seal the beaker
3) Sonicate for 5 minutes
4) Remove substrate from beaker and dry under a stream of nitrogen gas
5) Use immediately, or store under vacuum

Applying photoresist to substrates

1) Using hot plate, heat substrate to 95 °C
2) Turn on spin-coater and input settings (500rpm for 30 seconds)
3) Place clean substrate on the sample holder, and turn on vacuum pump
4) Using dispensing tube filled with photoresist (), cover the substrate surface with a layer of photoresist
5) When ready, start the spin-coating process using the settings programmed in step 2
6) Once complete, remove the substrate from the spin-coater and place on the hot plate (95 °C) for 2 minutes to cure. During this time, cover the substrate with an aluminum foil dome to prevent dust from settling on it.
7) After the 2-minute curing time is over, remove the substrate from the hot-plate and allow it to cool under an aluminum foil dome.
8) Shut down the spin-coater and clean
9) Once cool, the substrate is ready to use. Sore under vacuum if not used immediately

Sputter deposition on substrate (specific to AJA International, ATC Orion 5)

1) Attach substrate onto the removable stage using a small piece of tape on each side
2) Load substrate and stage into the sputtering machine, close lid, and tighten the lid. Ensure the vent valve is in the “closed position”. Adjust the stage height to the desirable height (I used 40)
3) Turn on chiller, and open cooling loops (temperature should be set at 16 °C)
4) Turn on main power switches and vacuum pump
5) Press “open”, and the chamber will begin to pump-down

6) Wait until chamber pressure reading displays “0 mTorr”, and check that the green interlock light is on
7) Open the gas valves on the argon and oxygen cylinders
8) If using argon:
    a. Open the argon flow valve, and turn to select the desired flow rate (in sccm)
9) If using oxygen
    a. Open the oxygen flow valve, and turn to select the desired flow rate (in sccm)
10) Open the rotation valve, and turn to “max” (should be 80 rpm) to ensure that the sample rotates during deposition
11) Press “set-point 1” and increase the value to 40
12) Twist the target knob to open the cover protecting the target when not in use
13) Turn power on for the RF power supply
14) Set the “load” and “tune” dials to the appropriate values (load=47 and tune=83)
15) Increase power to desired value (55W for Cu_2O, 83W for Al)
16) Press the “on/off” button, and immediately view the “reflected power” reading
17) If reflected power is greater than 0W, press the “on/off” button to turn it off, and adjust the load/tune dials
18) Repeat steps 16 and 17 until a reflected power value of 0W is achieved
19) Begin timer for the deposition time (this value will dictate the layer thickness)
20) When the deposition time is finished, immediately hit the “on/off” button to turn off the power to the target
21) Turn off RF power supply
22) Close the gas flow values on the machine, turn the rotation valve to 0 rpm
23) Hit “close” on the main controller, and then turn off power switches to the sputtering machine and vacuum pump
24) Close the gas valves on the cylinder
25) Turn off the chiller, and close the corresponding cooling loops
26) When ready, open the vent valve, and let the chamber slowly fill with air until atmospheric pressure is reached
27) Adjust the stage height to the maximum height above the bottom of the sputtering chamber
28) Open the chamber lib and remove the samples
29) Immediately use the samples, or store in vacuum until ready for use

Removing structure from photoresist-covered substrate

1) Place the substrate, with the sputtered and photoresist layers on it, in a jar
2) Fill with acetone until the substrate is fully covered, and seal the jar
3) Let it sit overnight

4) Using tweezers, remove the substrate, and use acetone to rinse off the sputtered thin-film into the jar
5) Allow thin-film flakes to settle, and then remove as much acetone-photoresist-mix as possible with a pipette
6) Add more acetone to rinse
7) Repeat steps 5 and 6 until all the photoresist has been removed (acetone should be clear)
8) The damp flakes can be scooped into a pellet mold, and dried under vacuum

Using the pellet mold

1) Clean and assemble the pellet mold
2) Remove the center pin
3) Load the damp thin-film flakes into the mold until it is full
4) Replace the center pin and apply pressure (by hand, or using a press to ensure the same pressure is achieved for each sample)
5) Disassemble the pellet mold, and carefully remove the fresh pellet
6) Dry pellet in vacuum oven until ready to use

Appendix B

XPS Reference for Copper and it's Oxides

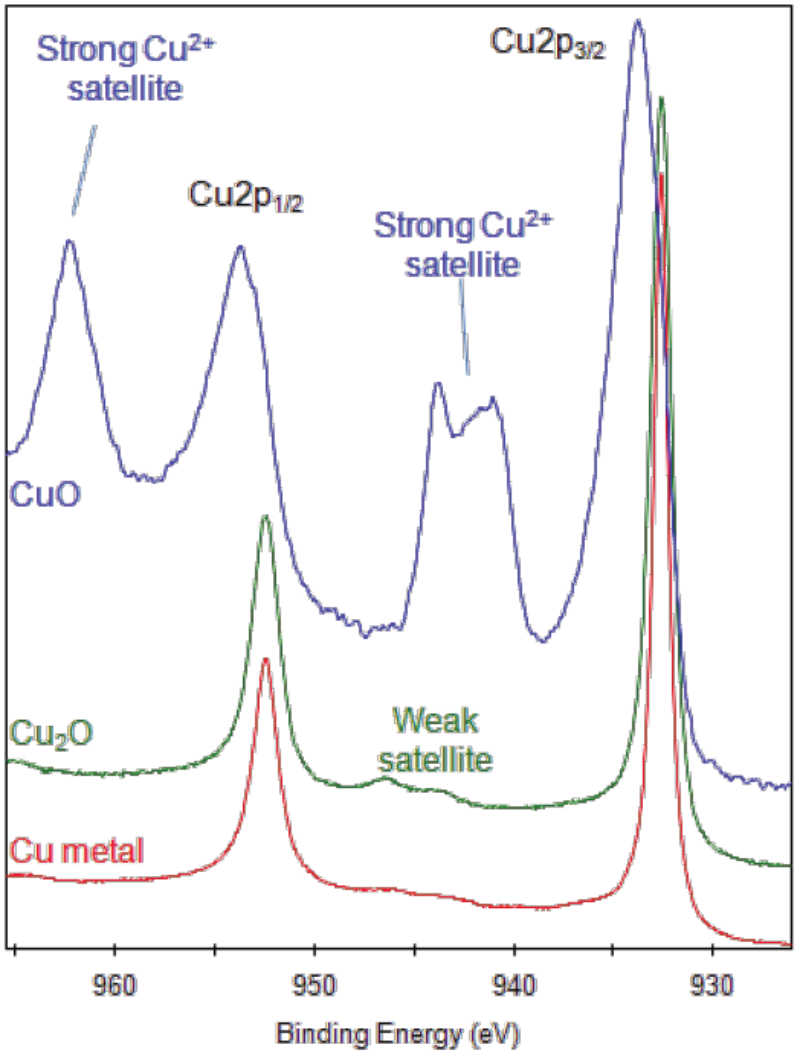

Image from Thermo Fisher Scientific Inc. [62]

Appendix C

Samples for Laser Ignition Testing

Sample	Cu_2O thickness (nm)	Al thickness (nm)	Ignition delay (us)	Average delay (us)	std dev
1	54	45	280	256	51.84593
			304		
			184		
2	54	15	312	274.6667	32.87687
			280		
			232		
3	54	90	340	330	21.60247
			350		
			300		
4	10	45	688	618.6667	76.54773
			656		
			512		
5	27	45	392	381.3333	20.99735
			352		
			400		
6	80	45	280	260	16.32993
			260		
			240		
7	107	45	510	589.3333	58.65909
			608		
			650		